

**The Present and Future  
Performance of the IRIS  
Spectrometer as Determined by  
Monte Carlo Simulation**

Mark A. Adams

ISIS Facility, RAL, CCLRC

## **Abstract**

Accurate Monte Carlo simulations of the high resolution inelastic neutron scattering spectrometer, IRIS, have been carried out using the neutron scattering virtual instrument tool, Vitess. The current configuration of the instrument is found to be non-optimal with a mismatch between the foci of the curved graphite analyser array and the positions of the corresponding detectors. The simulations predict that an improvement of a factor of two in detected neutron flux with an accompanying improvement in resolution can be achieved by remedying this situation. The effect of employing different supermirror guide configurations has been investigated and significant improvements in the neutron flux incident on the sample can be achieved. However, this is at the expense of a degradation in beam divergence, particularly at longer wavelengths. The simulations were very cpu intensive and for the first time a GRID-computing approach was employed to demonstrate that cpu times could be dramatically shortened for this type of simulation work. Some comments and recommendations for the future of the IRIS instrument are made.

## IRIS - Introduction

IRIS<sup>1 2</sup> is the highest resolution inelastic neutron scattering spectrometer at the pulsed spallation neutron source, ISIS. It was one of the initial suite of instruments available when ISIS began operation in 1985 and has undergone a number of changes during the last 20 years. This commitment to continual improvement has kept IRIS at the forefront of neutron science. It has consistently been one of the most over-subscribed instruments at ISIS, reaching over-subscription factors of between 6 and 7 in the mid 1990's, and over 400 publications have been produced as a result of work carried out on IRIS. In order to maintain its position as one of the world's leading neutron instruments it is essential to follow this path of continual improvement. To strengthen the case for attracting the necessary funding it is necessary to quantify the improvements that can be made by carrying out a full Monte Carlo simulation of the instrument. This report details the preliminary part of that work.

## IRIS - The Spectrometer

In its current configuration the neutron beam is transported down to the instrument along a 36.5m long neutron guide constructed from box-sections of natural-nickel-coated glass substrates. The neutrons scattered from the sample are then energy-analysed by Bragg reflection from either one of the two single crystal arrays (highly oriented pyrolytic graphite and muscovite mica). The spectrometer can therefore be considered to consist of two sections: a primary spectrometer (fig. 1) consisting of a long flight path over which the neutron pulses generated by two neutron disk choppers disperse, providing the time component of the resolution function and the secondary spectrometer (fig. 2) containing the crystal analyser arrays and the detector-banks.

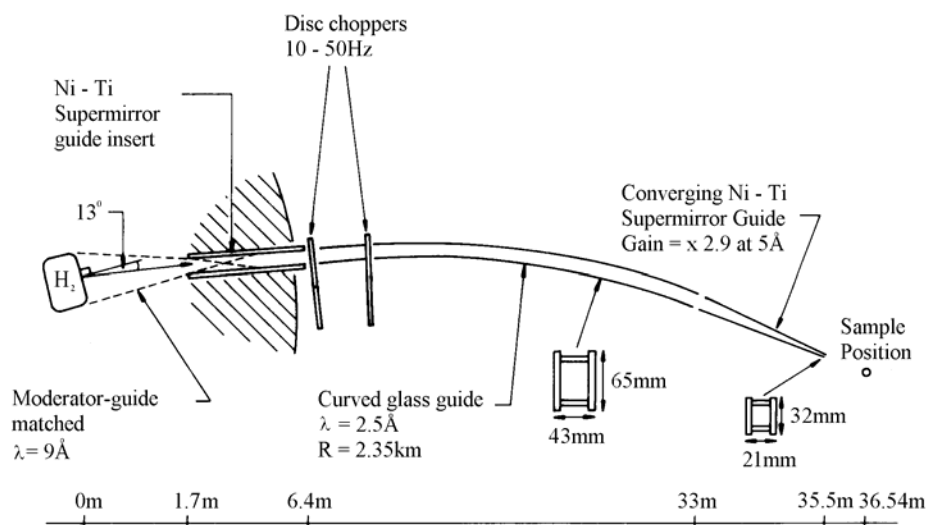


Figure 1. The IRIS Primary Spectrometer

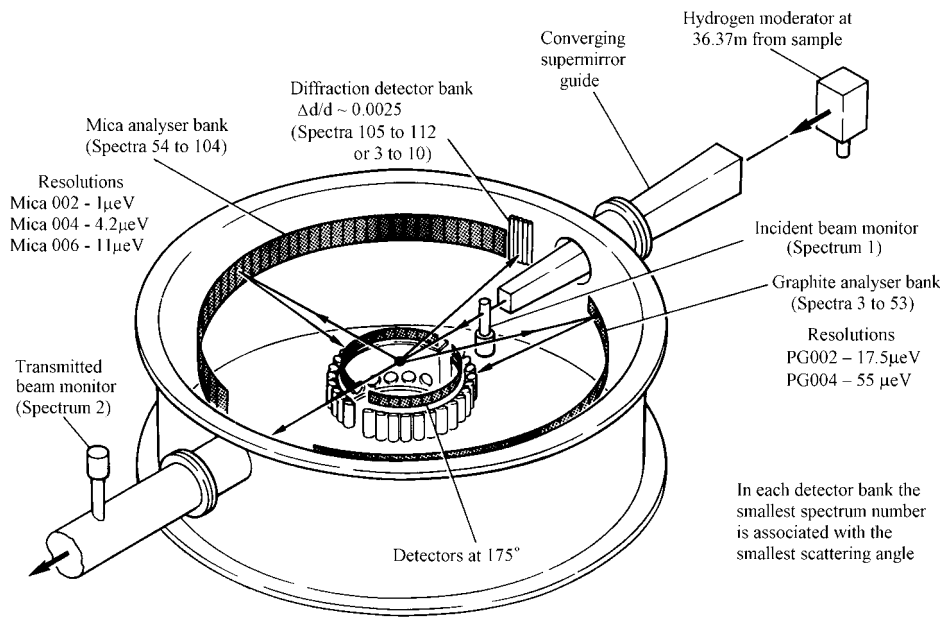


Figure 2. The IRIS Secondary Spectrometer

Using the two neutron beam choppers present in the incident flight path it is possible to select a particular neutron wavelength band. This allows the experimentalist access to a variety of different Bragg reflections; each with their associated energy-resolution, energy-transfer ranges, momentum-transfer ranges, intensity and signal-background. IRIS is thus an extremely versatile neutron scattering spectrometer and the broad range of science covered on the instrument reflects this. The more usual instrument settings are shown in table 1 which shows clearly that although the mica analyser options provide for much improved resolution and access to lower Q-values they suffer from a lack of intensity. This is due to an inherently lower incident flux of long wavelength neutrons and lower reflectivities for the mica reflections c.f. the graphite reflections. One of the ways this situation could be improved is by using an alternative to the muscovite mica such as fluorinated mica and this possibility has been addressed in some detail<sup>3</sup>. Another approach to the low count-rate for the mica analyser reflections is to improve the neutron flux incident on the sample with the use of supermirror neutron guides. This will also have a beneficial impact on the graphite analyser reflections.

The efficiency of the beam transport along the neutron guide is strongly dependant on the reflectivity of the inner surfaces of the neutron guide. When comparing reflectivities in this context it is usual to express them in terms of an "m-factor" where m=1 refers to the reflectivity of natural nickel. When IRIS was constructed there were only two alternatives available, natural nickel and <sup>58</sup>Ni with an m-factor of 1.2. Since then, the development of thin supermirror coatings consisting, for example, of alternating layers of nickel and titanium, has led to m-factors of 4 becoming available. This has already been demonstrated to be an effective means of improving instrument performance. One of the many

Table 1. Standard Inelastic Settings on IRIS for the pyrolytic graphite (PG) and muscovite mica (M) reflections

Analyser reflection and Intensity relative to PG002	Resolution (FWHM) at elastic line ( $\mu\text{eV}$ )	Chopper operating frequency	$\Delta E$ (meV)	$\Delta Q_{\text{elastic}}$ ( $\text{\AA}^{-1}$ )
PG004 (0.7)	55.0	50	-3.5 to 4.0	0.844 to 3.719
PG002 (1.0)	17.5	50	-0.4 to 0.4	0.422 to 1.859
PG002 (1.0)	17.5	50	-0.2 to 1.2	0.422 to 1.859
PG002 (0.5)	17.5	25	-0.8 to 0.8	0.422 to 1.859
PG002 (0.33)	17.5	16.7	-1.0 to 10.0	0.422 to 1.859
M006 (0.4)	11.0	50	-0.4 to 0.4	0.396 to 1.864
M004 (0.15)	4.5	50	-0.15 to 0.15	0.264 to 1.263
M002 (0.04)	1.2	50	-0.02 to 0.02	0.132 to 0.621

improvements that IRIS has undergone has been the installation of an  $m=2$  supermirror converging guide section at the end of the primary flight-path to increase the flux per unit area at the sample position (by a factor of 2.8). In addition, when the OSIRIS instrument <sup>4-7</sup> was installed during the late 1990's the front-end of the neutron guide within the target station shielding (shared by both instruments) was upgraded to an  $m=2$  supermirror guide. This improved the flux on IRIS by about 20%. It is clear that large flux gains can be made, which will have an impact on all users of the instrument, by replacing the natural nickel-coated sections of glass guide with supermirror-coated guide. A comparison of the measured fluxes on IRIS and OSIRIS, sharing the same beam port but with OSIRIS having  $m=2$  supermirror guide all the way from the target-station to the sample position, indicates that gains in flux of at least a factor of 2 are envisaged for IRIS. However, in order to determine the optimal supermirror guide configuration for an improved IRIS it is necessary to turn to Monte Carlo simulation.

## Monte Carlo Simulation of Neutron Scattering Instrumentation

Rather than calculating the performance of neutron instruments by hand a number of instrument simulation codes have been developed, based around the Monte Carlo technique. The most popular of these are Vitess <sup>8</sup> and McStas <sup>9,10</sup>.

In this work the program Vitess has been used and this was for a variety of reasons. In its original incarnation as the Monte Carlo Data Reduction technique it

was used as a means of analysing the line-shape of the helium roton signal observed on IRIS <sup>11</sup>. From this rather specific application it has been developed into a useful multi-functional simulation tool with much of the impetus (and necessary funding) for this provided by the European Spallation Source project <sup>12</sup>. Vitess has been used to simulate many different types of neutron instrument but from the beginning there has always been an emphasis on providing the necessary modules, such as neutron guides and crystal analyser arrays, needed to simulate long flight path inverted geometry spectrometers such as IRIS. It is more user-friendly than McStas and simulation set-up times are generally acknowledged to be shorter. Another important factor in the choice of Vitess as the simulation tool was that it was important to be able to compare this work with previous simulations of IRIS and most of these have been done using Vitess.

## **Computing Aspects of the Simulation Work**

Vitess can be run on both Unix and Windows machines but most of the simulations were carried out under the Linux operating system on a 2.4 GHz AMD dual-processor machine (equivalent to a 3 GHz Intel Pentium). The use of a dual processor machine enabled two simulations to be run at the same time. Simulations of the primary spectrometer required  $1 \times 10^9$  neutron trajectories and took between 5 and 12.5 hours. The complete instrument simulations required  $3 \times 10^9$  neutron trajectories in order to achieve the necessary statistical quality. The simulation of the current instrument configuration took 12 hours and the higher m-factor simulations required up to sixty-six hours of cpu time. In a previous simulation study <sup>13</sup> it was stated that simulations with 50 billion neutron trajectories took between 4 and 8 hours on a 3 GHz Intel processor (c.f. the 200 hours estimated from this work). A close investigation of the parameters used in the previous study revealed a number of errors which could account for some of the difference but not for a factor of between 25 and 50. With no other information being made available apart from the report itself it has to be assumed that 50 billion is a typographical error.

## **Simulations of the Current IRIS Spectrometer**

The first task in any instrument simulation work is to produce a model of the instrument which accurately reproduces the current performance of the said instrument. It is only by doing this, reproducing observed data, that we can be confident in using the simulation to predict how the instrument will perform after improvements have been made. As a pre-cursor to this it is necessary to acquire the details of the instrument design and construction. The information on IRIS was obtained from a number of sources. Some engineering drawings were available and copies of the more important ones used in this work are shown in Appendix A. In conjunction with this, personal knowledge, based upon many years of association with the instrument, was used extensively and the actual position, size and shape of some of the beam-line components were determined by physical measurement. Some of the information provided in previous studies was also used if deemed reliable and accurate.

## Pipes

Vitess enables the user to construct a complete instrument from source to detector as a series of individual modules joined together in the form of a pipe – a computing concept which is common to both the UNIX and Windows operating systems. A number of screenshots showing the details of the more important modules are to be found in Appendix B. The complete instrument simulation consists of the following modules: source (hydrogen moderator), m=2 straight neutron guide section, 1<sup>st</sup> disk chopper, m=1 curved neutron guide section, 2<sup>nd</sup> disk chopper, long stretch of m=1 curved neutron guide, m=1 straight neutron guide section, m=2 converging guide section, sample, graphite analyser bank and finally detector. In addition, a number of beam monitors and output modules are included at various points along the pipe for diagnostic and data output purposes. Some of these modules will now be discussed in detail.

## Hydrogen Moderator

The spectrum of neutrons from the hydrogen moderator is represented by a data file called Vit.Iris containing both the time and wavelength distribution of the neutron flux (fig. 3). This has been produced at ISIS using the MCNPX code developed at Los Alamos (<http://mcnpx.lanl.gov/>). Unfortunately, the code ‘blows up’ at certain wavelengths producing spurious features (fig. 4). This is not important if the simulation is concentrated upon a limited wavelength range around, for example, the PG002 reflection, but for simulations of the instrument investigating the effect of using supermirror guides over a wide range of wavelengths it is a problem. A simple way round this is to split the file into its component parts (time and wavelength) by integration and fit the wavelength component (which is the part which contains the spurious feature) by a doubly-decaying exponential function (fig. 5). Vitess is capable of accepting these two separate files as a representation of the flux distribution from the source and this is what was used for the primary spectrometer simulations. The original, and slightly more accurate, Vit.Iris file was used for the simulation of the complete instrument over the limited wavelength range of the PG002 reflection.

## Neutron Guides

The most important parameter within the guide modules is the name of the reflectivity file which contains the reflectivity profile (reflectivity as a function of incident scattering angle) of the particular coating used. The reflectivity profiles used in these simulations are the standard ones contained within Vitess (fig. 6). No attempt was made to use those provided by the various neutron guide manufacturers. In addition, more sophisticated guide options such as parabolic focussing guides<sup>14,15</sup> were not considered as they are not a standard option within Vitess. Obviously, when it is time to purchase the neutron guides further simulation work should be considered as there is some variation between manufacturers and customised guide coatings and geometries are also a possibility.

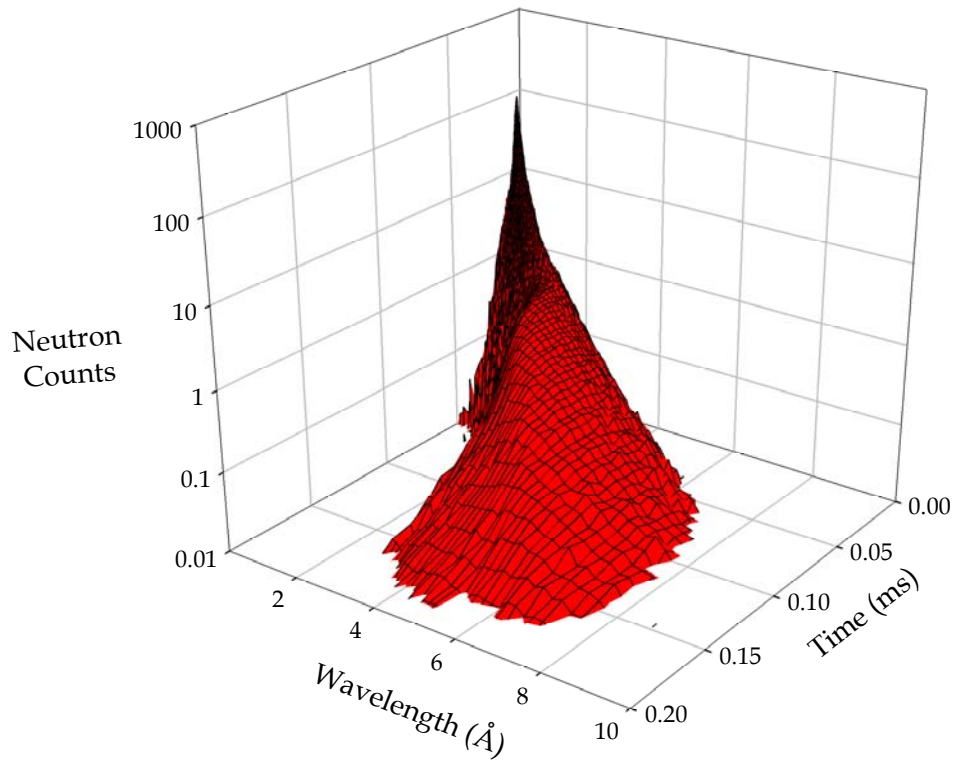


Figure 3. Vit.Iris Neutron Flux Distribution (log scale)

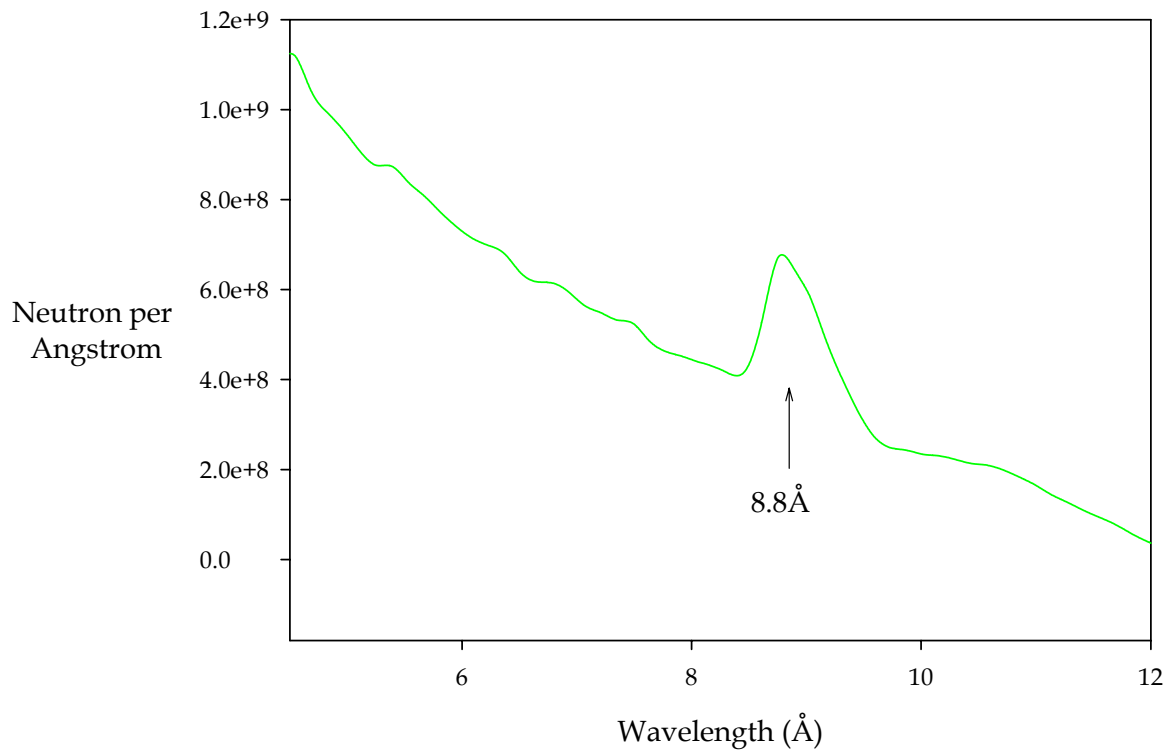


Figure 4. The spurious feature at 8.8Å

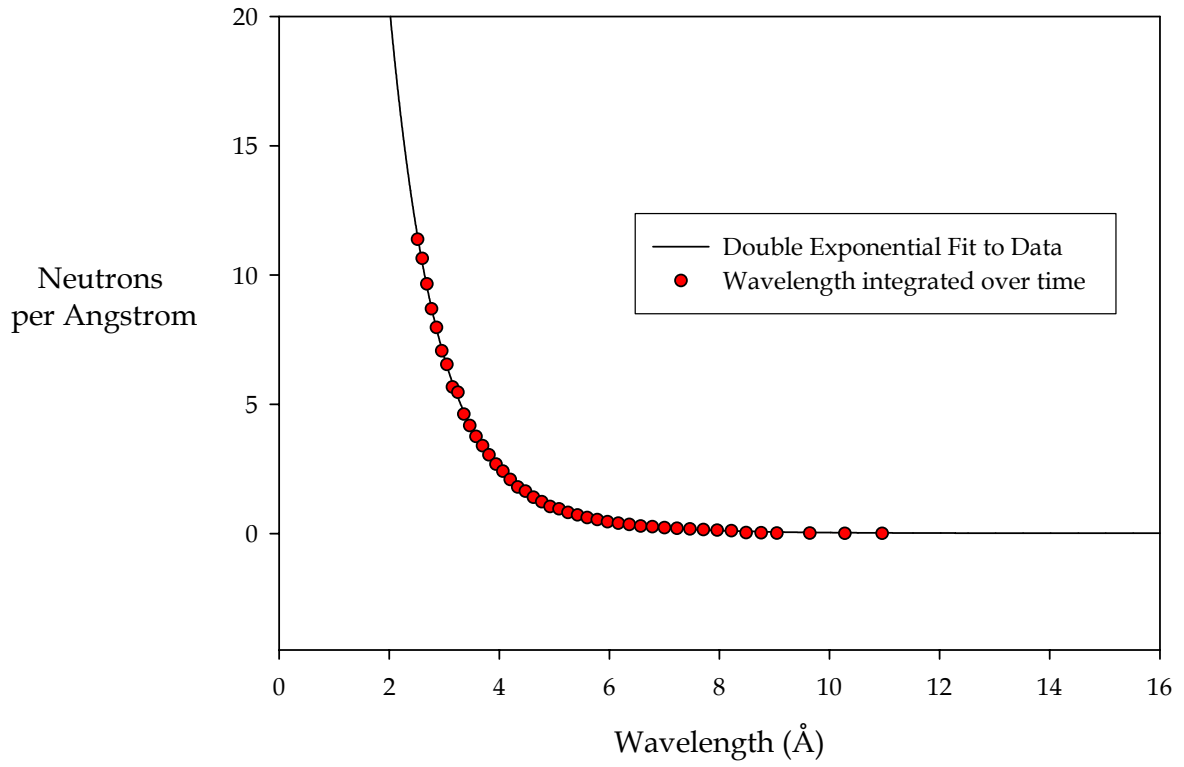


Figure 5. The fitted wavelength distribution file

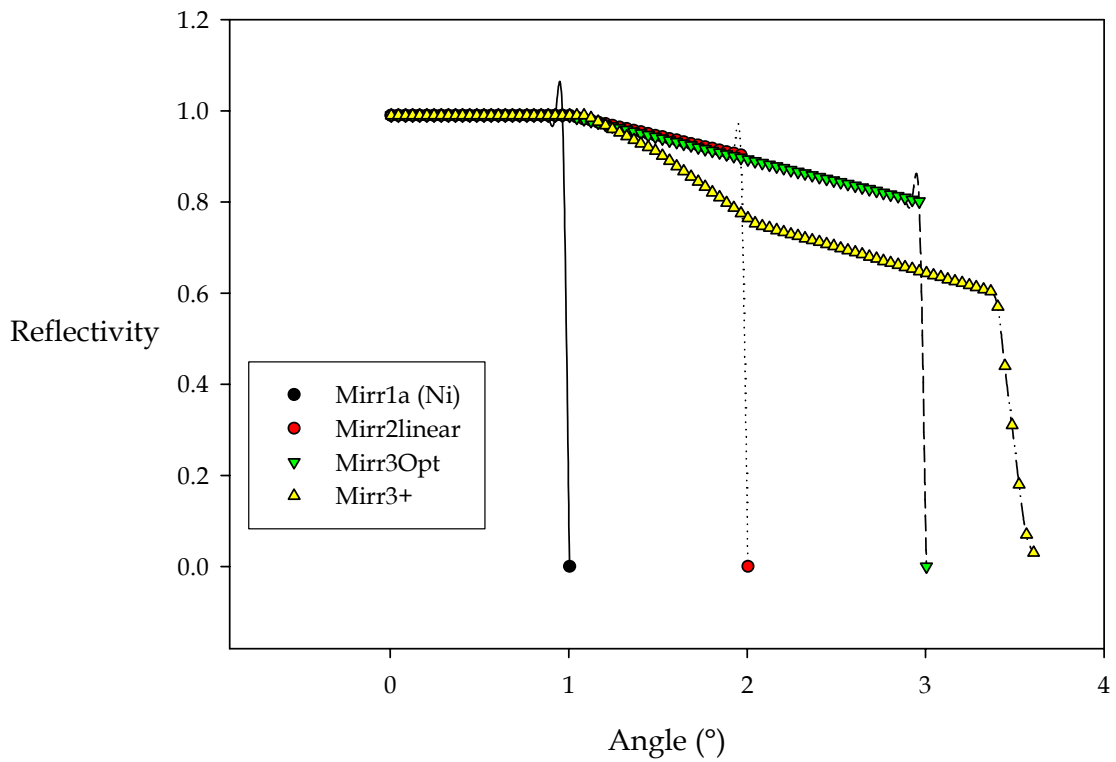


Figure 6. Reflectivity profiles for the standard guide coatings in Vites

## Vitess Description of the Graphite Analyser Bank

The monochromator-analyser module in Vitess requires a very specific format for the co-ordinates and orientation of the crystals forming the analyser bank (in this work, the graphite analyser bank). Firstly, a position on the bank must be defined as the nominal centre and then the values of the Cartesian co-ordinates of this nominal centre need to be specified (relative to some origin - the sample position being the most convenient). The positions of the other crystal elements (CE) are then given in terms of deviations from this position i.e. ( $\Delta X$ ,  $\Delta Y$ ,  $\Delta Z$ ). Similarly the orientations given by the angles  $\theta$  and  $\phi$  of both the crystal surface and the Bragg planes of the crystal at this central position are also given. Note that  $\theta$  and  $\phi$  conform to the Eulerian rotation system but with  $\omega$  unused (fig. 7) and that the reason for separating out the crystal surface and Bragg angles is to allow for the possibility of off-cut crystals i.e. crystals in which the Bragg scattering planes are not co-planar with the surface of the crystal. The orientations of all other CE's within the analyser bank are then also expressed in terms of deviations from these "main surface" and "Bragg" offset angles. The calculated positions and orientations for the crystals of the IRIS analyser bank are represented in figures 8 and 9 and can be compared with the engineering drawings in Appendix A. It is very important to get this correct. In one of the previous IRIS simulation studies<sup>13</sup> the main surface offset angle was given as  $0^\circ$  and the Bragg offset angle was  $4.96^\circ$ . This describes a situation in which the Bragg scattering planes of the highly oriented pyrolytic graphite crystals are off-cut relative to the surface of the crystals by  $4.96^\circ$ . This is an incorrect description of the graphite analyser bank. Furthermore, the angle specified implies that the neutron beam is deflected by an angle of  $9.92^\circ$  which on the real instrument (as will be shown later) would not intersect with the detectors.

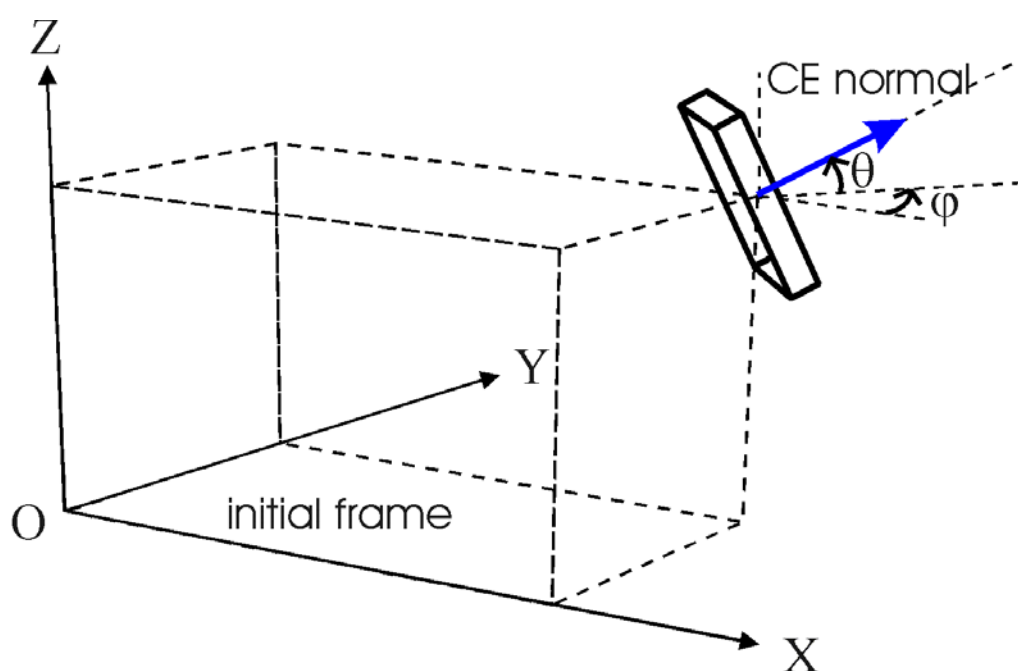


Figure 7. The definition of  $\theta$ ,  $\phi$  and Eulerian Rotation (from the Vitess user manual)

The original IRIS paper <sup>1</sup> states that the scattering angle (sample-analyser-detector) on IRIS is  $175^\circ$  which suggests that for the Vitess specification the main scattering angle should be  $2.5^\circ$   $((180-175)/2)$ . Whilst producing the co-ordinates of the graphite crystals it was observed that the main surface offset (and hence Bragg) scattering angle at the appropriate position on the current analyser bank is  $3.9^\circ$  which means that the neutron beam is being deflected by an angle of approximately  $7.8^\circ$  (corresponding to a scattering angle of  $172.2^\circ$ ). This is inconsistent with the original IRIS concept and all available information regarding the position of the detector bank. The actual position of the detector bank has been measured and the centre of the detectors corresponds to a scattering angle of  $174.6^\circ$ . This means that there is quite a significant mismatch between the position of the IRIS detector bank and the centre of the reflected neutron beam. It is important to investigate this problem.

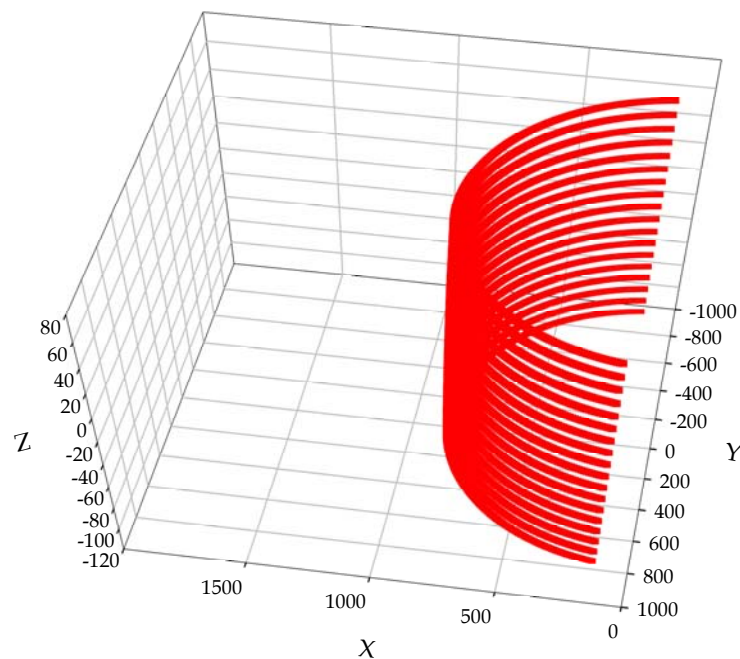


Figure 8. The Graphite Analyser Profile in Direction of the Incident Beam - Y

The original simulation work for the profile of the current analyser was carried out using Monte Carlo code developed in-house at ISIS many years ago, MCGUIDE <sup>16</sup> and MCLIB <sup>17</sup>. A great deal of work was involved in optimizing the analyser profile <sup>18,19</sup>. The offset angles and x,y,z co-ordinates for the central column of CE's produced from this work were made available <sup>20</sup> and they are different to the values for the current analyser. Clearly, at some point between the simulation work and the production of the engineering drawings the profile was changed. There is no evidence to suggest that the current analyser has not been constructed in accordance with the engineering drawings and so this implies that the currently installed graphite analyser profile is not optimal. Simulations have been carried out in order to determine the consequences of this.

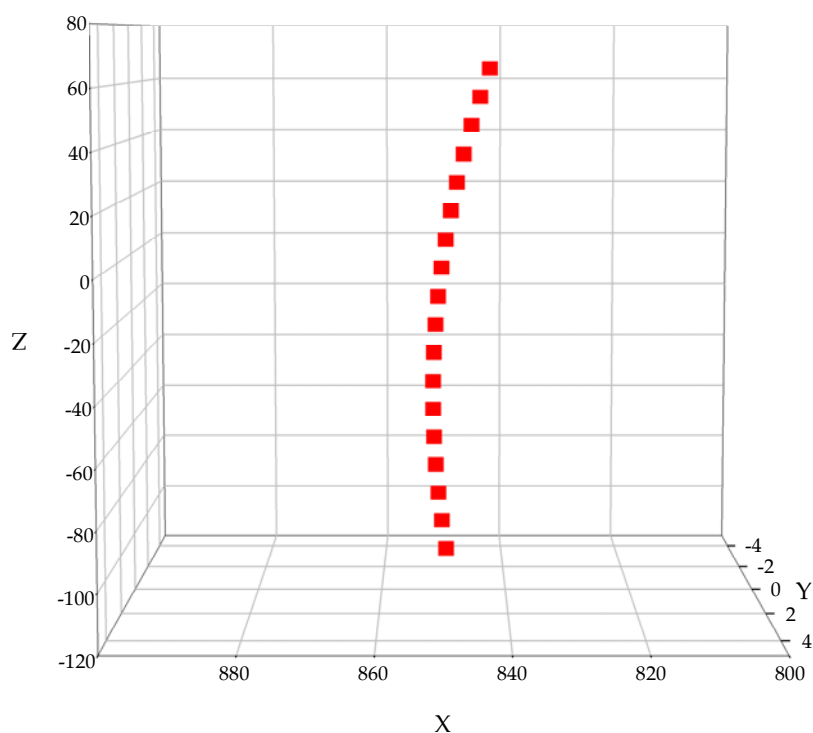


Figure 9. Close-up of profile at centre of analyser bank

## Results of Initial Simulations

The standard calibration sample used on IRIS is composed of three concentric vanadium cylinders of diameters 10,16 and 20mm. This is a purely incoherent scatterer which over a limited energy-transfer range is effectively an elastic scatterer and hence can be used to determine the resolution of the spectrometer. Figure 10 shows the simulated PG002 elastic line compared with the measured vanadium data (after being scaled to the simulated data). The agreement is excellent with, in addition, the error 'going the right way' i.e. the simulation, which is in many respects an idealised view of IRIS, indicates a slightly narrower resolution width than the real instrument. Immediately this confirms that the current analyser profile and instrument parameters are well-understood. Using this as the starting point the effect of the non-optimal analyser profile can be investigated. Figure 11 shows a comparison of the elastic lines for: the current analyser (simulated and measured – detectors at  $5.4^\circ$  below horizontal), the current analyser with the detectors dropped by 25mm (detectors now at  $7.8^\circ$  below horizontal which then should match the current analyser profile) and finally a fully optimised analyser/detector configuration with the detector at  $5.0^\circ$  and using the analyser profile determined from previous simulation studies<sup>18,20</sup>. Figures 12 and 13 show the same information in more detail.

The main conclusion to be drawn from this work is that the current detector bank is only intercepting half of the beam being reflected by the analyser. Interestingly, in the original simulation work<sup>18</sup> two possible analyser profiles were investigated. In one of these only half the reflected neutrons from the analyser were

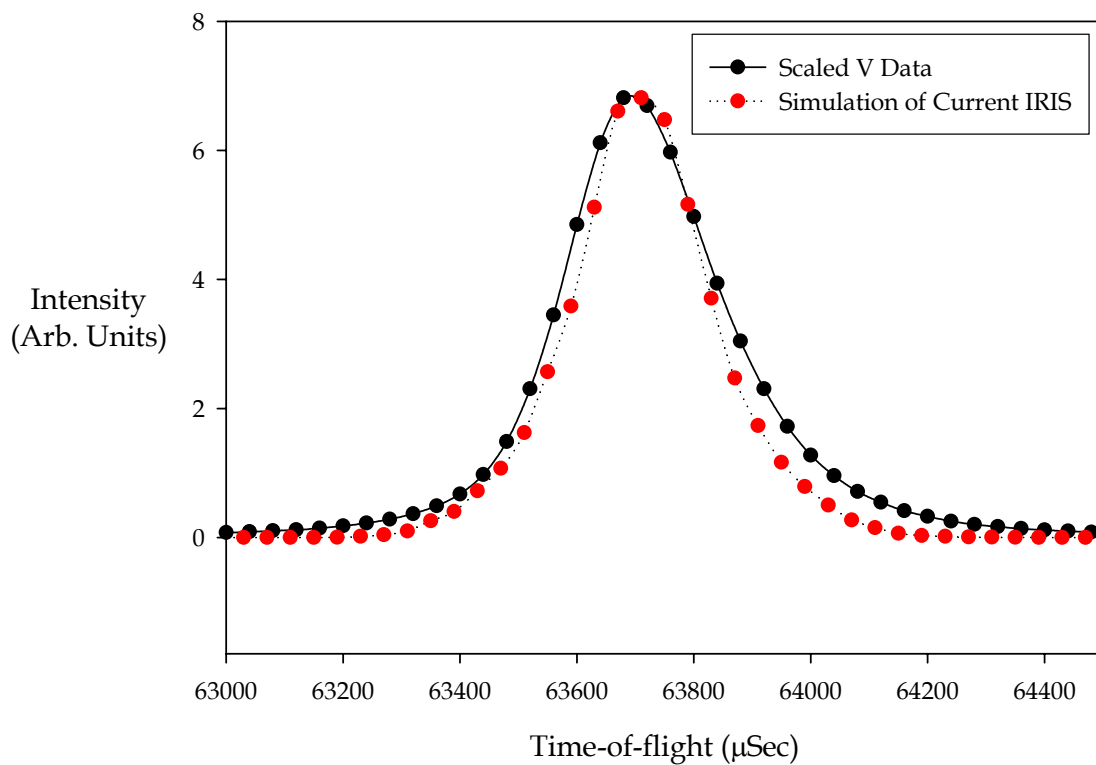


Figure 10. Comparison of the Elastic Lines - Simulated vs. Measured Vanadium Data

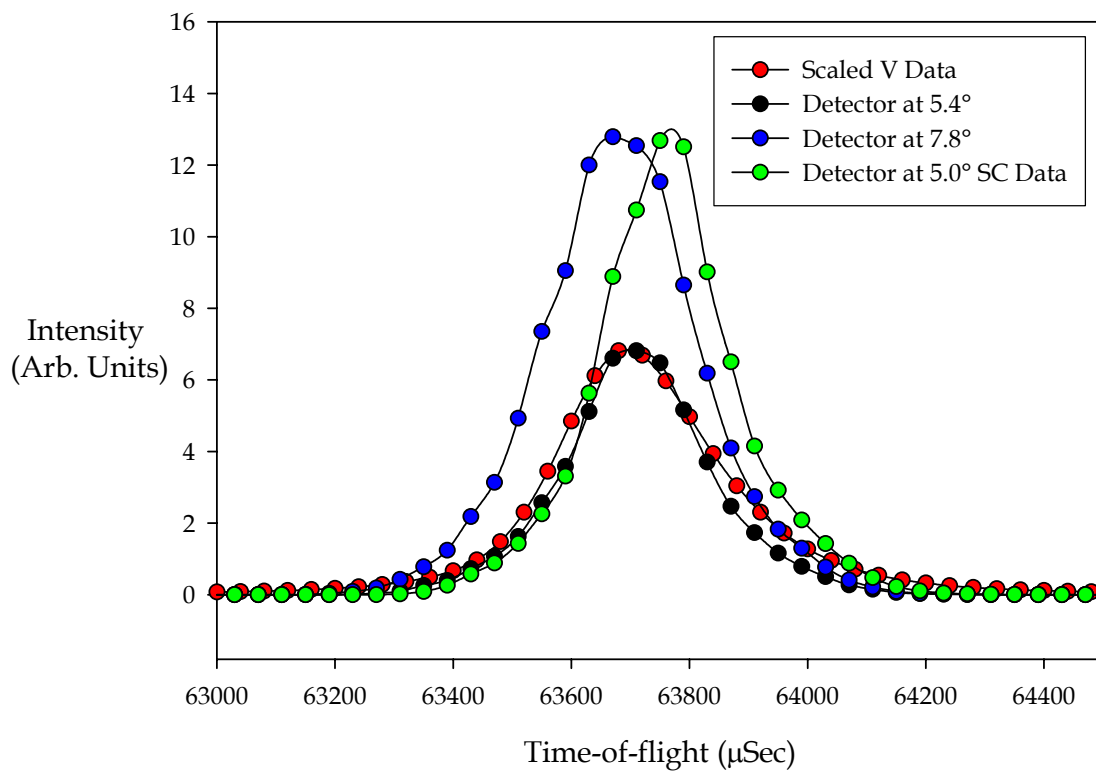


Figure 11. Effect of the non-optimal analyser profile

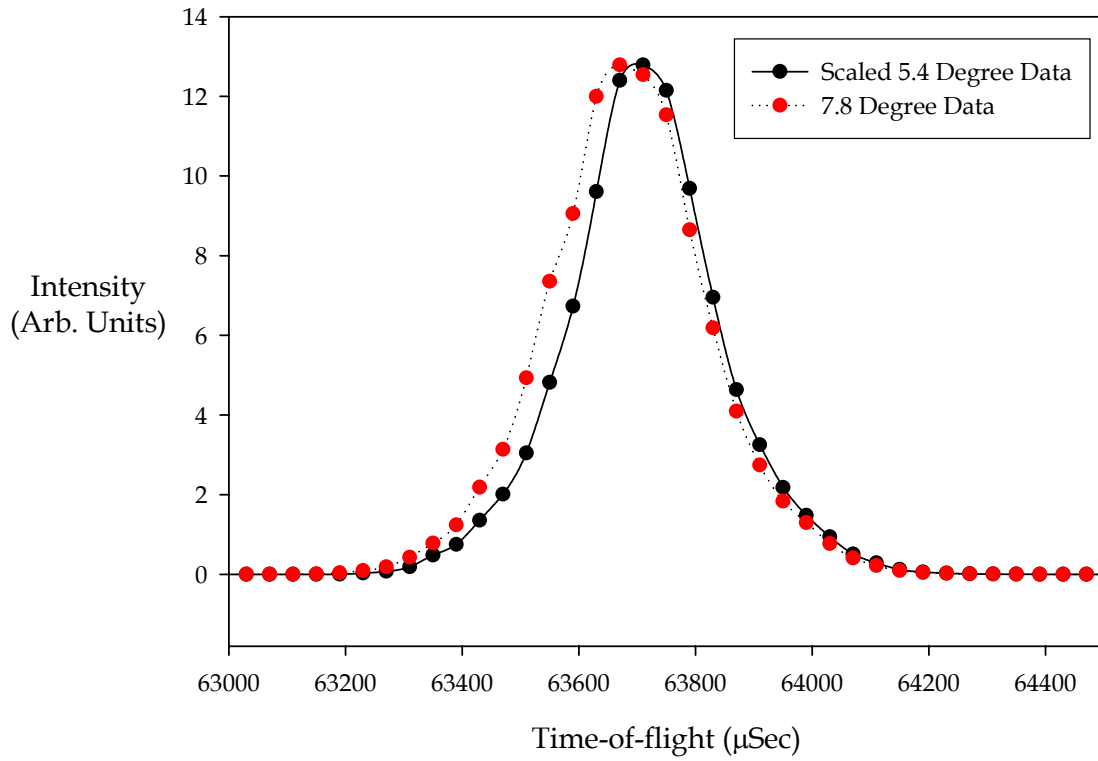


Figure 13. Comparison of Simulated Resolution Function with the Detector banks at Different Scattering Angles.

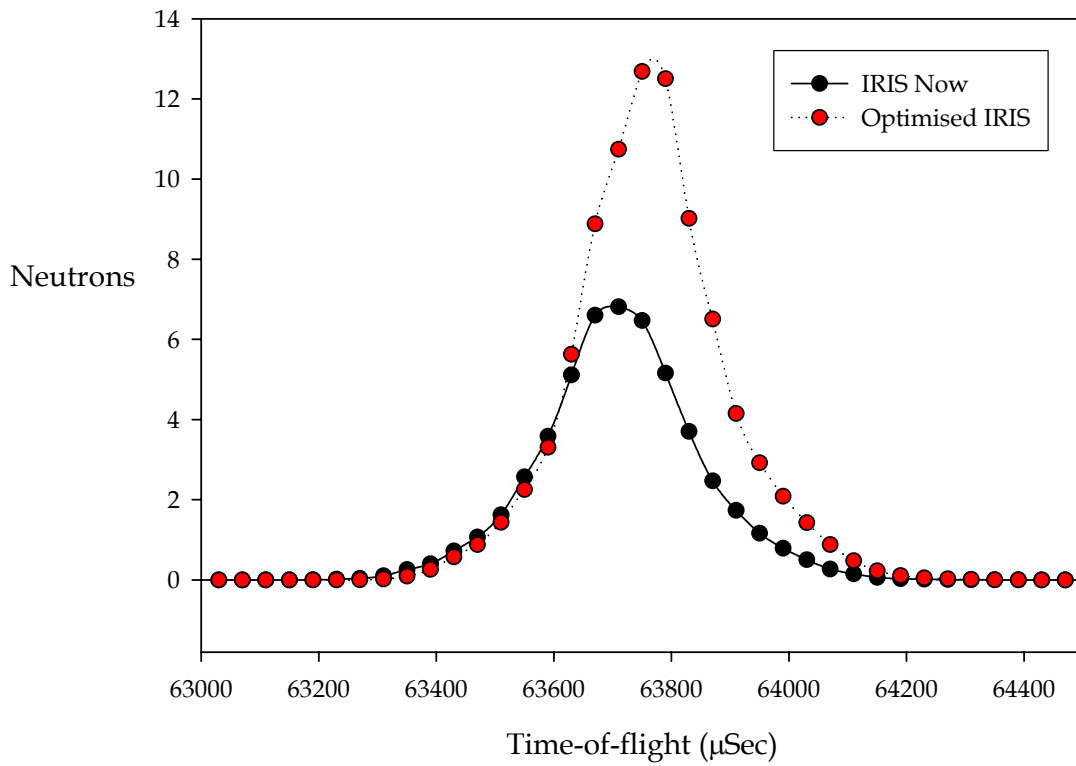


Figure 14. IRIS after analyser optimisation

intercepted by the detector and for this reason the other profile was chosen.

There are two possible ways in which this problem can be addressed. The analyser band could be re-manufactured (nominal cost £30-40000) or, as in the simulation, the detector bank could be dropped by 25 mm so that it intercepts the reflected beam fully giving a factor of two more neutrons but with a degradation in resolution by about 20%.

## Supermirror Configurations

Following the work needed to ensure that the current IRIS instrument is well understood it is now possible to investigate the effect of modifying the instrument. Initially, just the primary spectrometer was simulated in order to generate results quickly. Unfortunately, the size of the output files generated by Vitess precludes the possibility of splitting the simulation into two parts i.e. using the results from the primary instrument simulations and feeding them into the secondary spectrometer simulations so following the primary instrument simulations much longer simulations of the whole spectrometer were carried out. Both sets of simulations used a variety of supermirror configurations and the designations for each of the different configurations simulated are described in figure 15 and table 2.

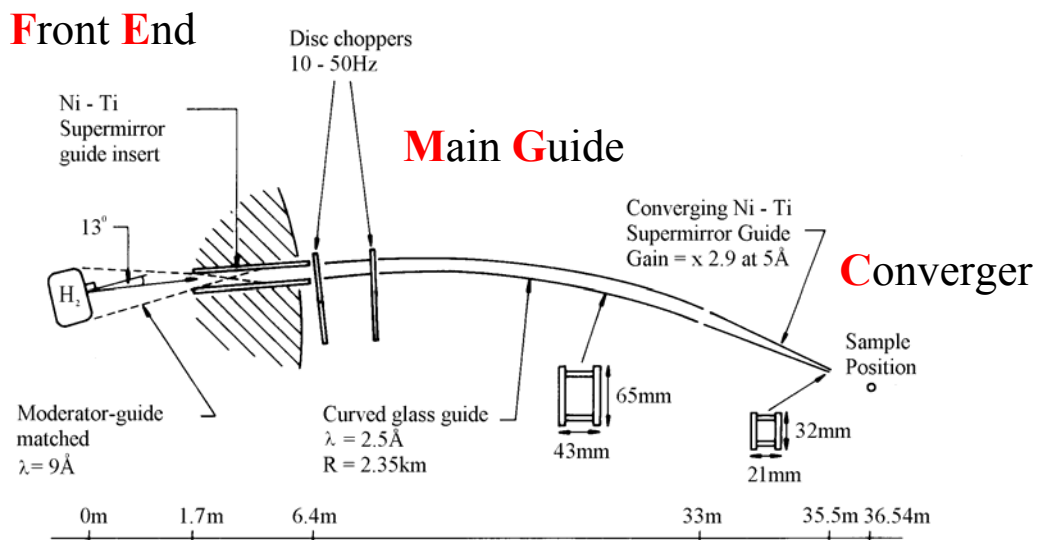


Figure 15. The three sections of the primary spectrometer changed in the simulations

## Primary Spectrometer simulations

In figure 16 the flux distribution as a function of wavelength for the various supermirror configurations simulated is shown. This indicates that the best configuration for increasing the neutron flux on IRIS is the P333 configuration with the P233 a very close second. The reason for the similarity of the P233 and P333 configurations is likely to be that within the target station shielding the neutron guides are straight and so the at the beginning of the curved section of guide after

Table 2. Simulated guide configurations

Simulation Description	Guide m-factors used in simulations		
	Front End	Main Guide	Converger
212	2	1	2
222	2	2	2
232	2	3	2
2352	2	3.5	2
233	2	3	3
333	3	3	3
23535	2	3.5	3.5
353535	3.5	3.5	3.5

the first chopper there is still a direct view of the moderator. Figure 17 shows the comparison between the higher m-factor mirror configurations and the current IRIS configuration as a series of ratios. Clearly, the most significant flux gains are to be had at shorter wavelengths. This is typical of the performance of supermirrors and is an important consideration for a new area of science currently being developed on IRIS which is the study of hydrogen. This work requires neutron energies up to 20 meV which are currently not available in large numbers. A factor of 8 improvement in the flux of these neutrons is significant.

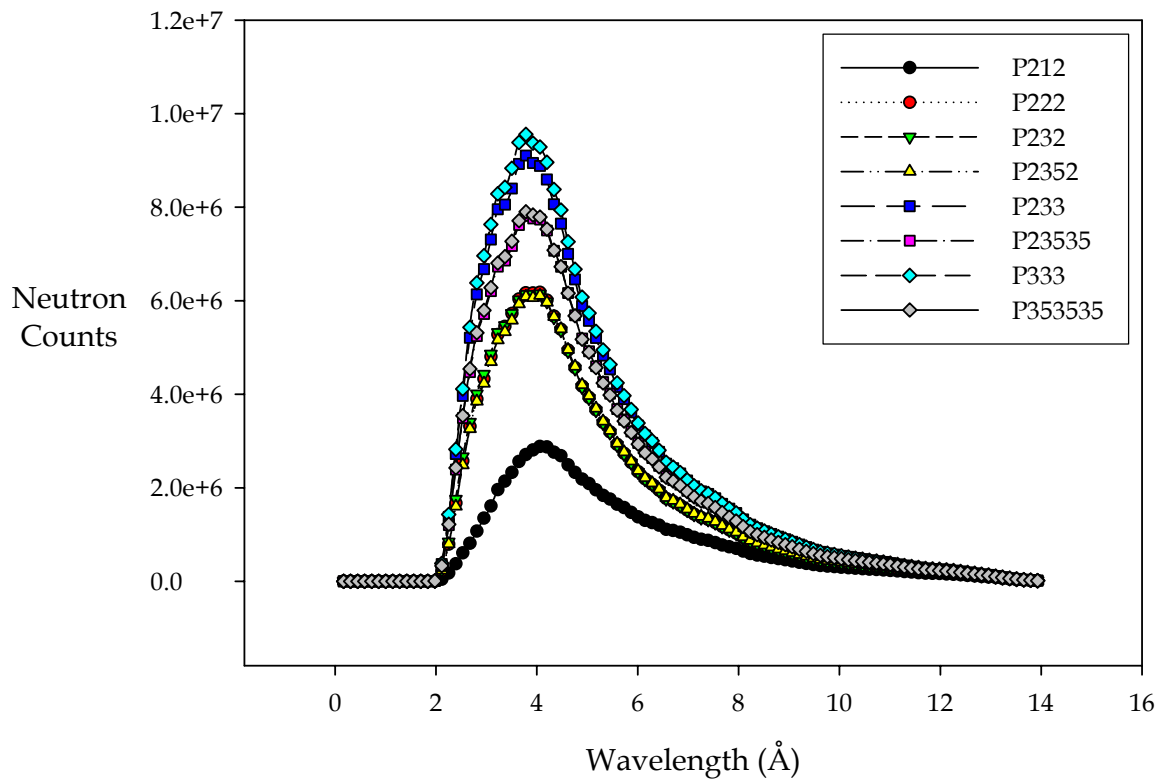


Figure 16. Flux distribution as a function of wavelength

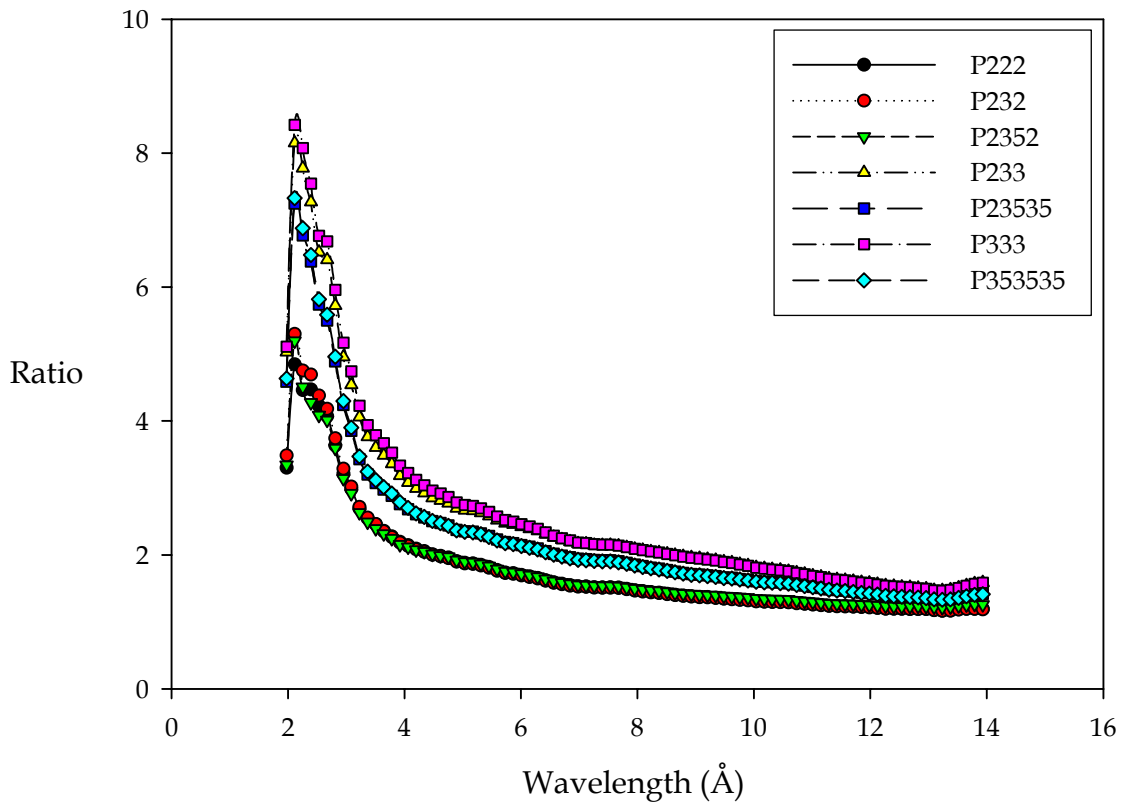


Figure 17. Relative wavelength ratios for the different configurations

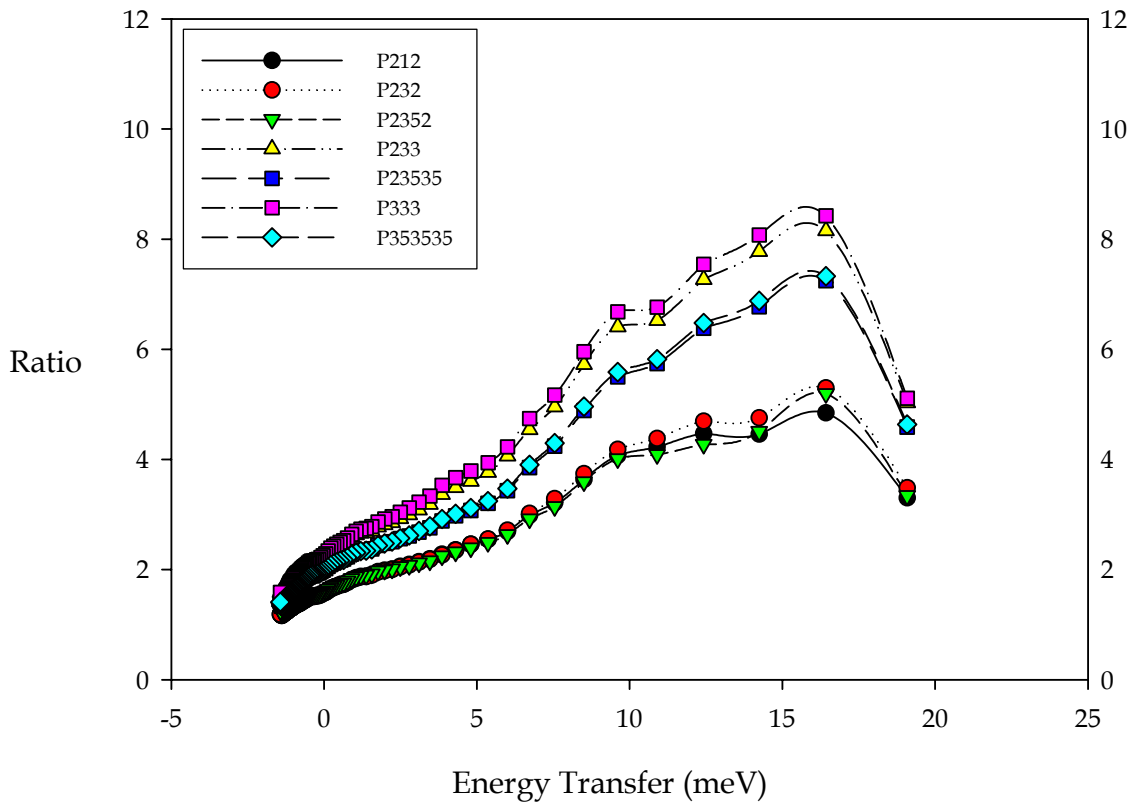


Figure 18. The ratios as a function of energy transfer (for PG002 reflection)

As well as the change in final neutron flux the change in beam profile for the different configurations is also important - neutrons which miss the sample do not contribute to anything other than background. In general, the beam profile at the sample position changes from pseudo-rectangular towards a more elliptical shape as the m-factors of the mirrors increase as a result of an increased beam divergence in both horizontal and vertical planes. Note that the profiles (figures 19 (a) - 19 (h)) are in order of detected neutron flux confirming again that the P333 configuration is superior to the other configurations. It's important to remember that this results from the reflectivity profile of the m=3.5 supermirror contained within Vites. A better optimised m=3.5 coating would yield different results.

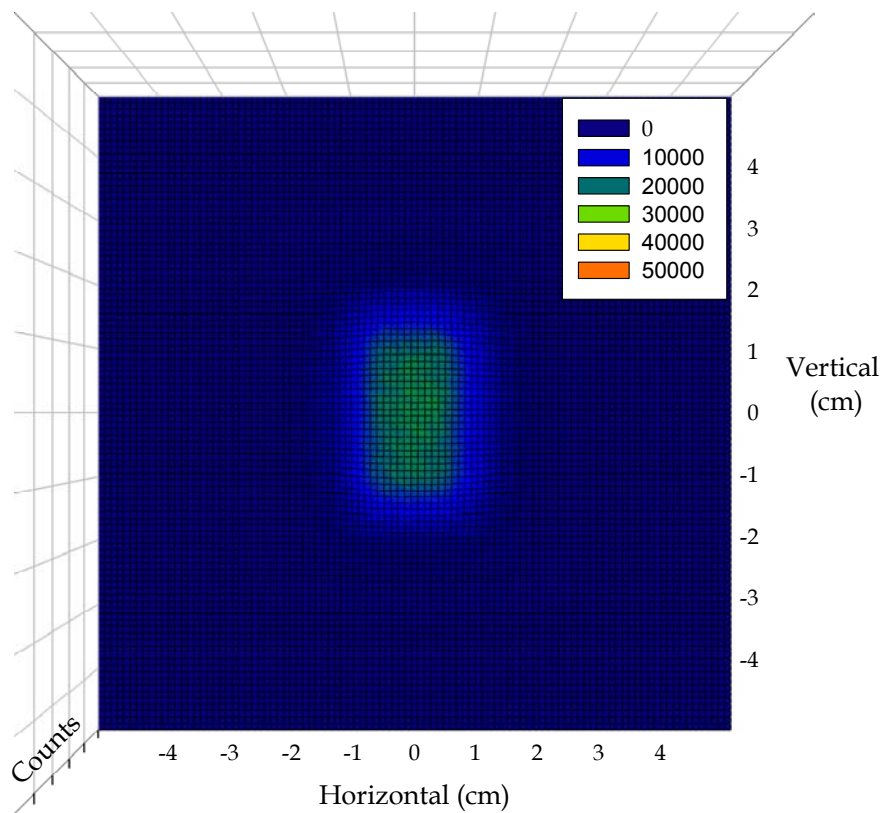


Figure 19(a). Beam profile - M212

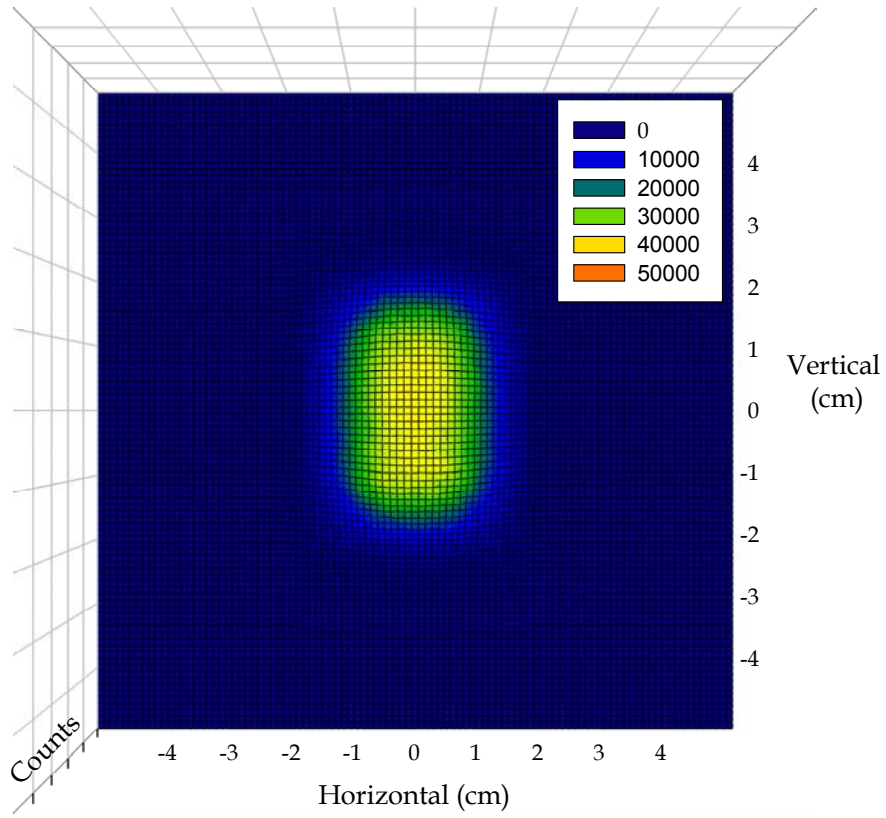


Figure 19(b). Beam profile - M222

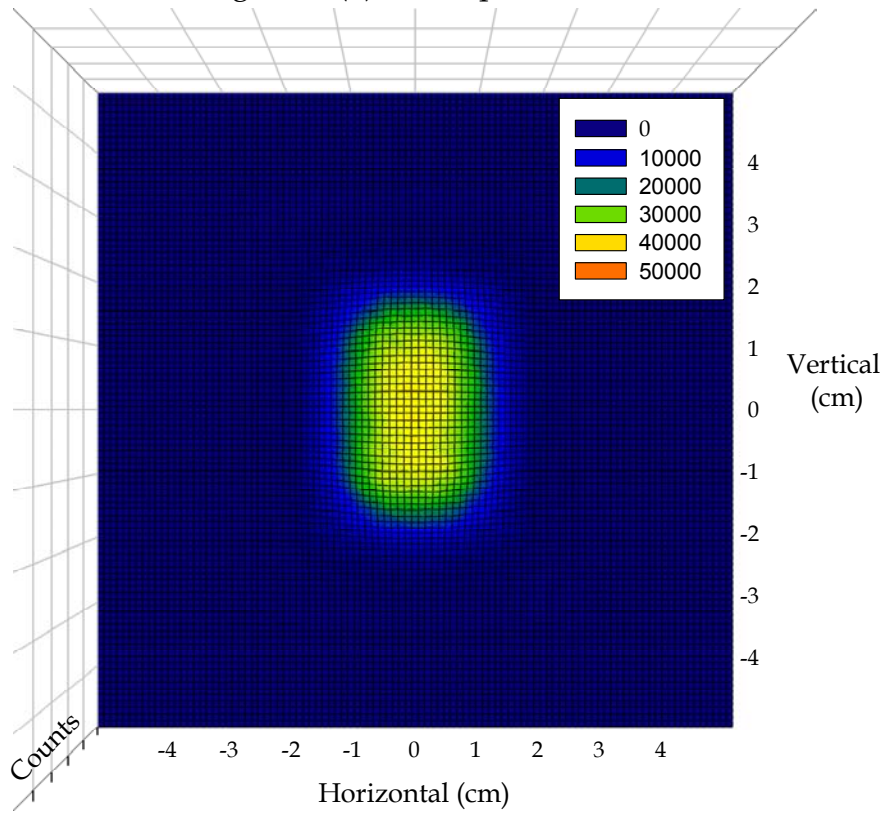


Figure 19(c). Beam profile - M232

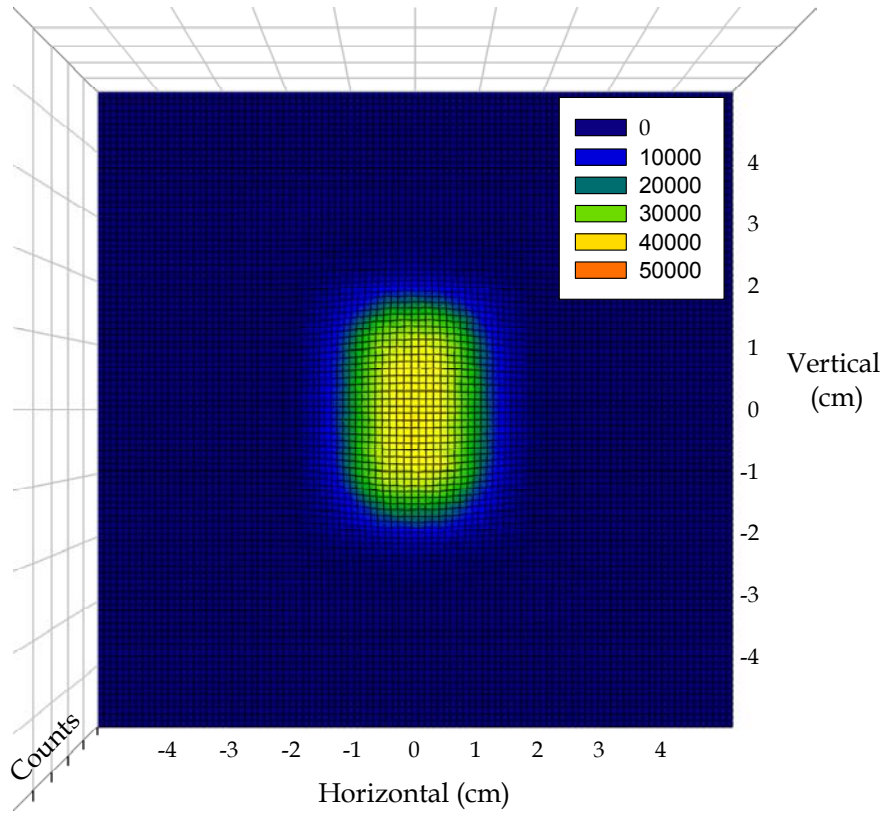


Figure 19(d). Beam profile - M2352

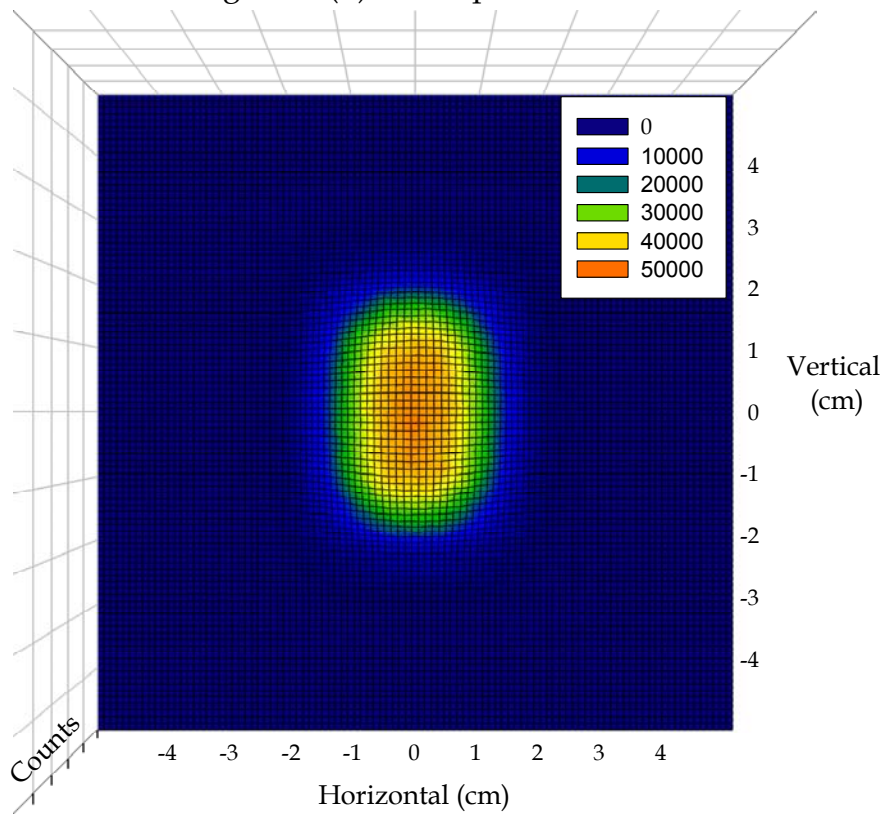


Figure 19(e). Beam profile - M23535

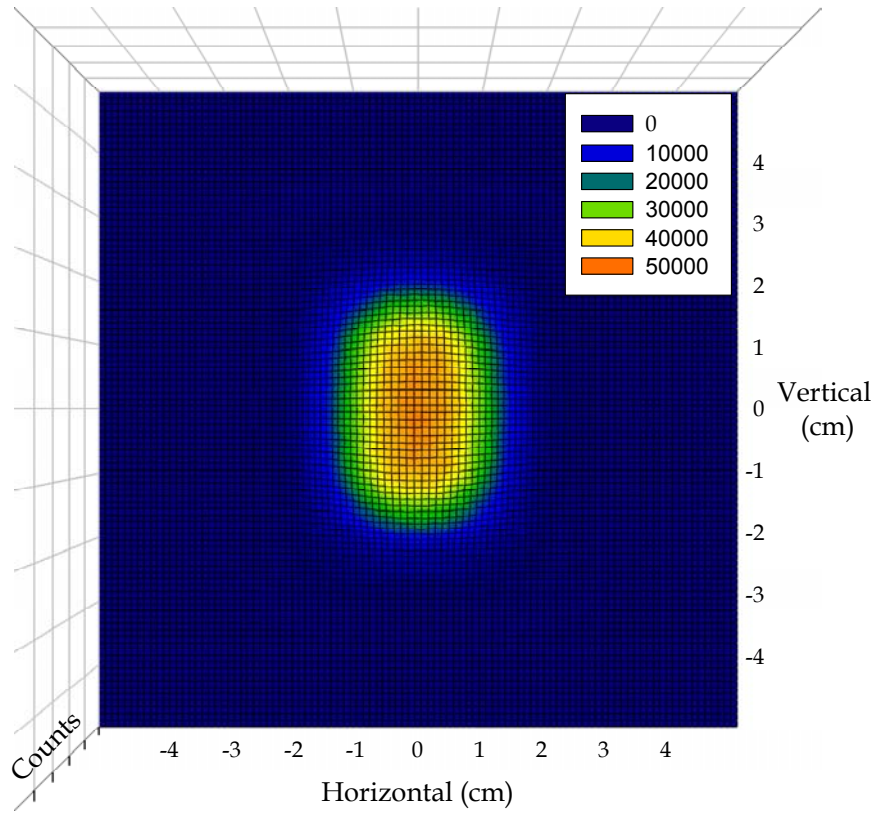


Figure 19(f). Beam profile - M353535

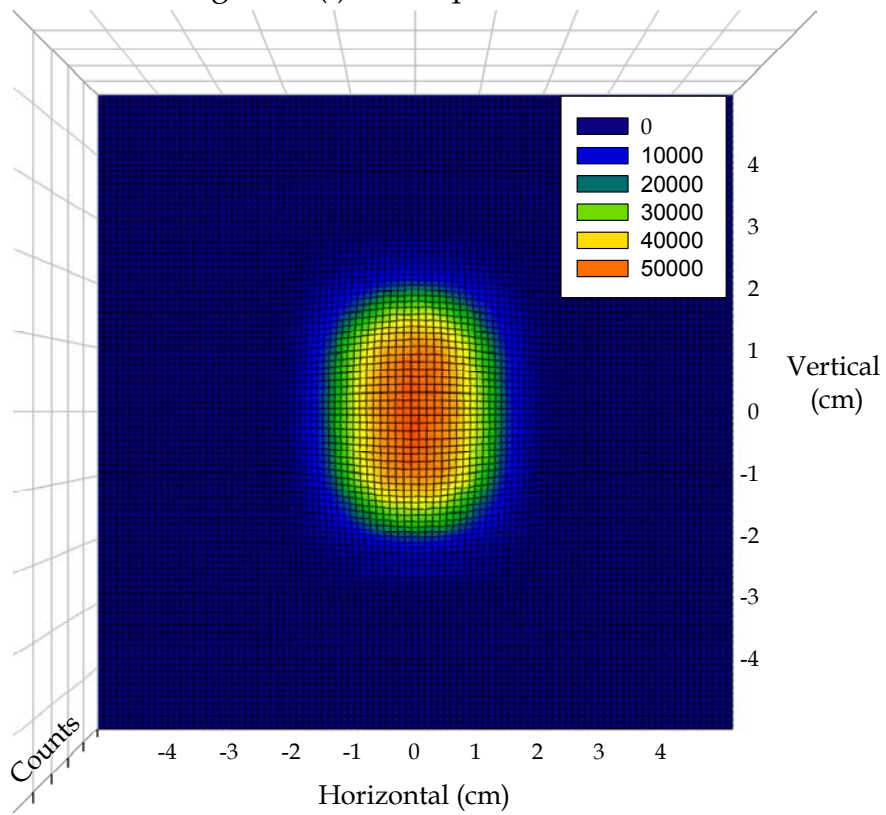


Figure 19(g). Beam profile - M233

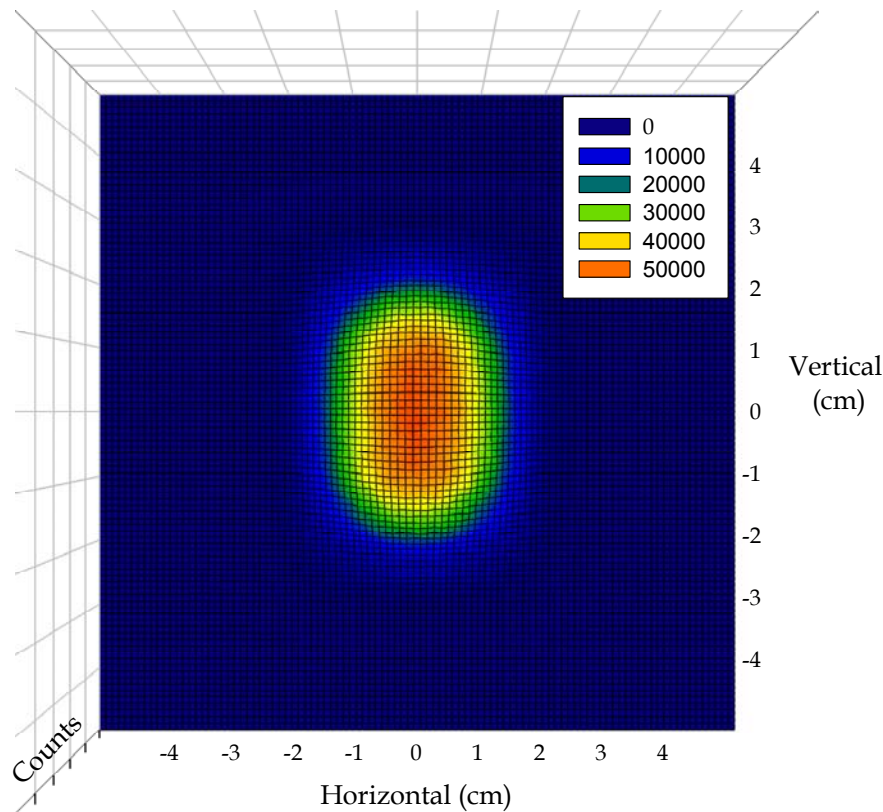


Figure 19(h). Beam profile - M333

The change in the beam divergence as the mirror m-factor is increased is illustrated in figures 20-27. Remember that in the co-ordinate system used, X is along the beam, Y refers to the horizontal axis and the Z-axis is vertical. The divergence plots show first of all that as the m-factors are increased then the divergence grows as expected. The beam divergence in the vertical plane is larger and more structured than in the horizontal plane. However, an effect of going to higher m-factors is, in both cases, to smooth out the peaks in the beam divergence at shorter wavelengths giving a more uniform distribution of beam divergence. Most of the neutrons are contained within the central sections of each divergence distribution with only a small fraction of neutrons contained within the side-lobes. For example, in the P212 configuration the beam divergence mainly lies between  $\pm 2^\circ$  in the horizontal plane and  $\pm 3^\circ$  in the vertical and for the P353535 configuration this increases to  $\pm 3^\circ$  and  $\pm 3.5^\circ$  respectively. The plots of divergence vs. wavelength show that the side-lobes come from the longer-wavelength neutrons which is why they are of low intensity. At longer wavelengths the beam divergence in both horizontal and vertical planes increases significantly. This is an important factor for the use of long wavelength neutrons on IRIS.

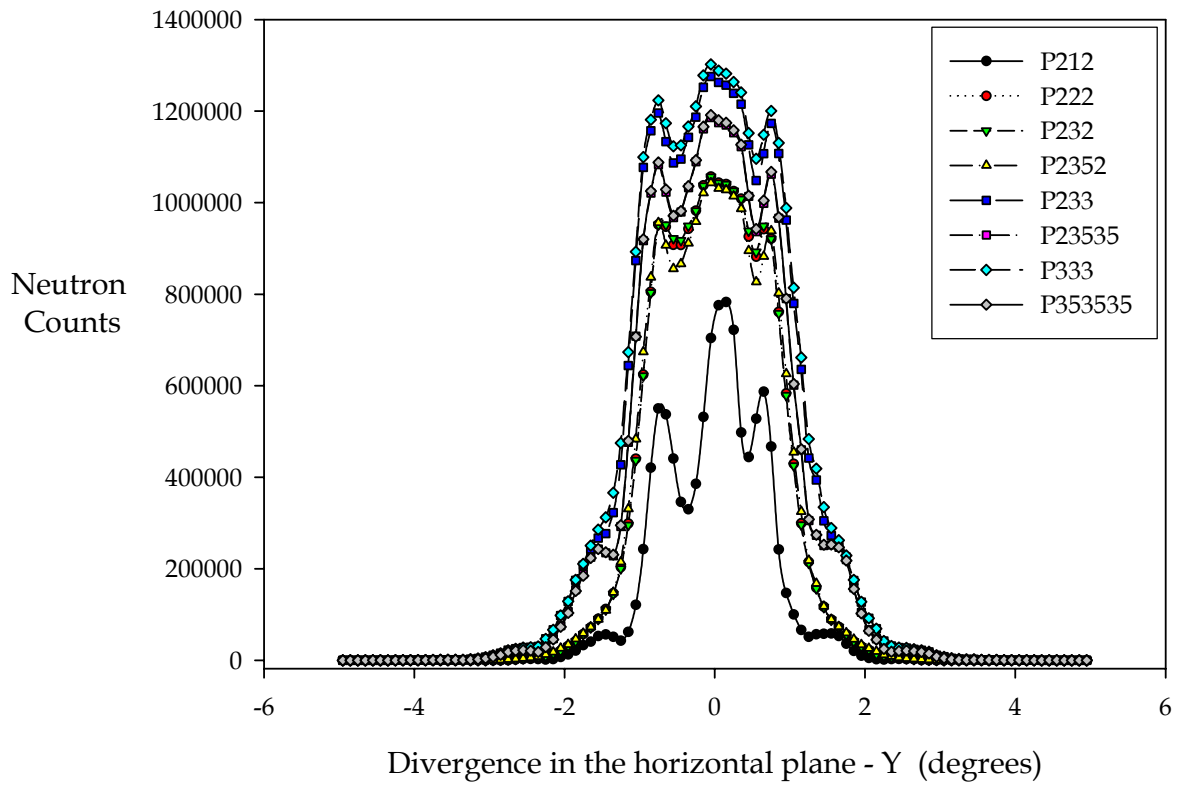


Figure 20. Horizontal beam divergence for all guide configurations

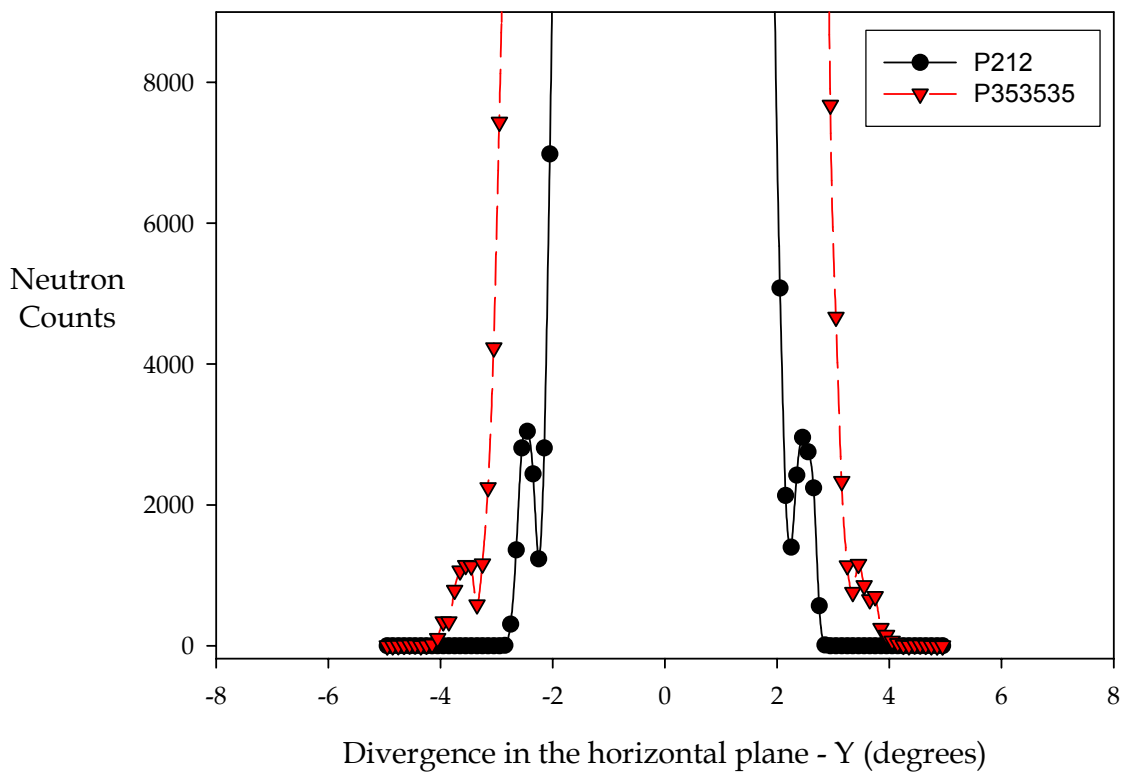


Figure 21. Horizontal beam divergence for P212 and P353535 – details at the base

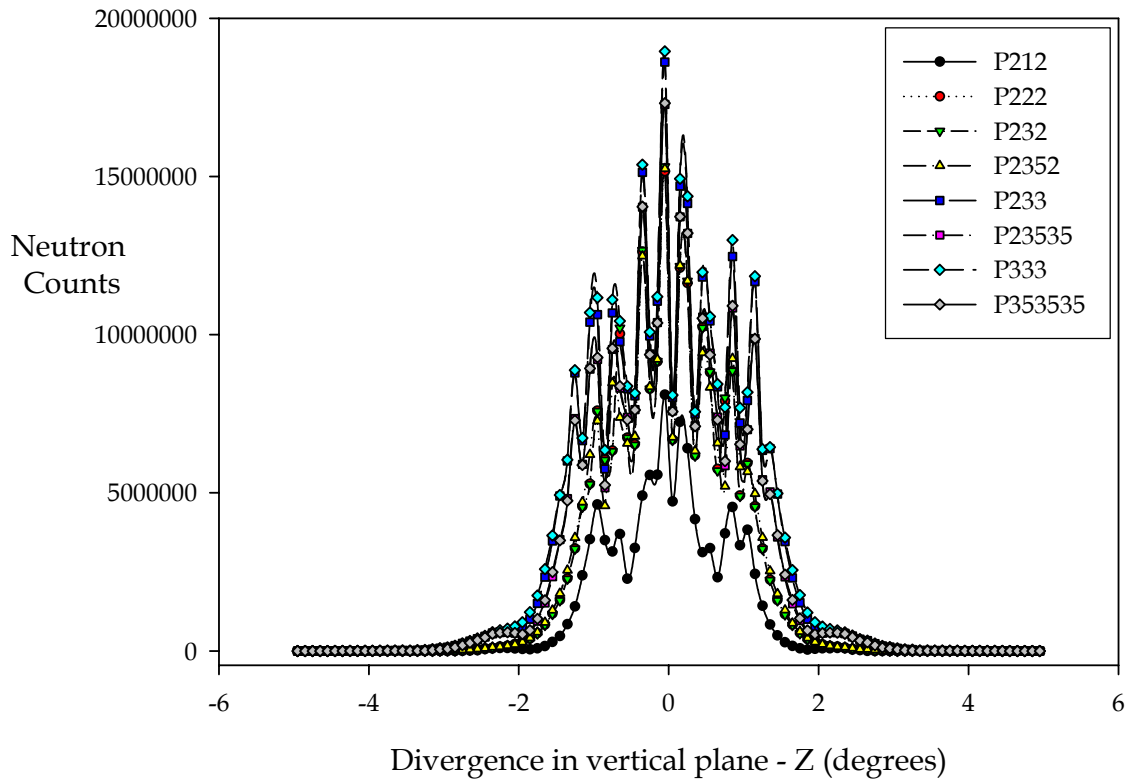


Figure 22. Vertical beam divergence for all guide configurations

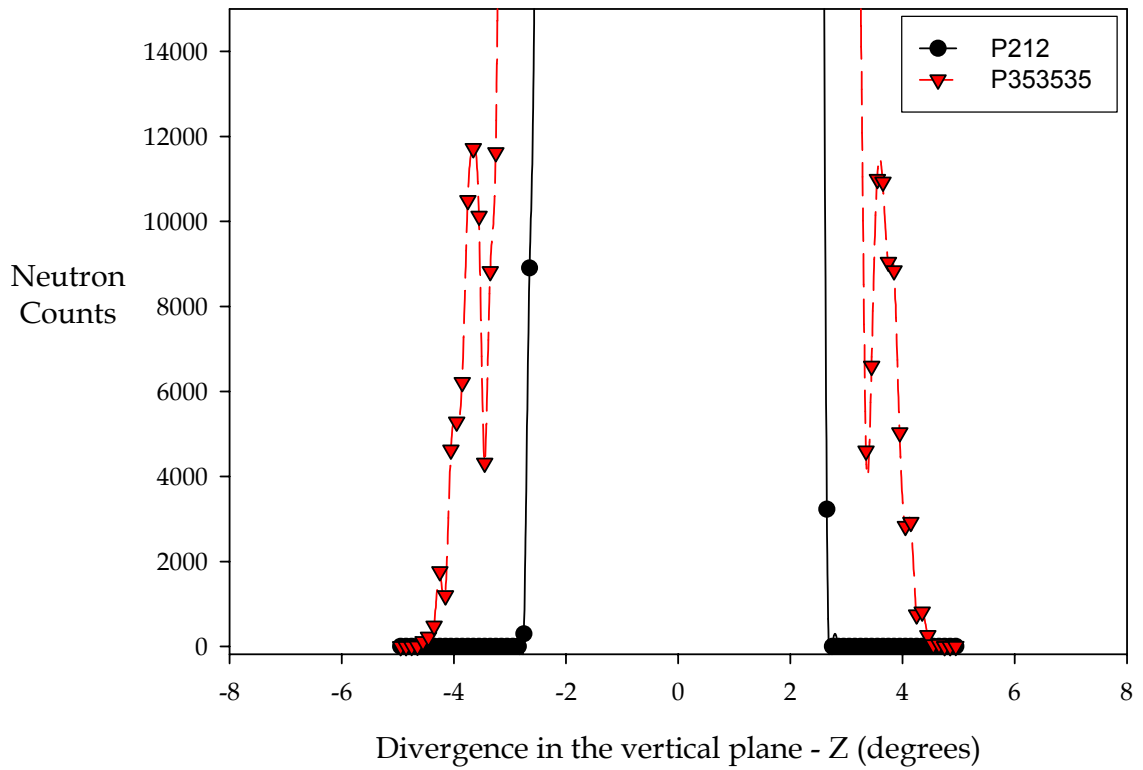


Figure 23. Vertical beam divergence for P212 and P353535 – details at the base

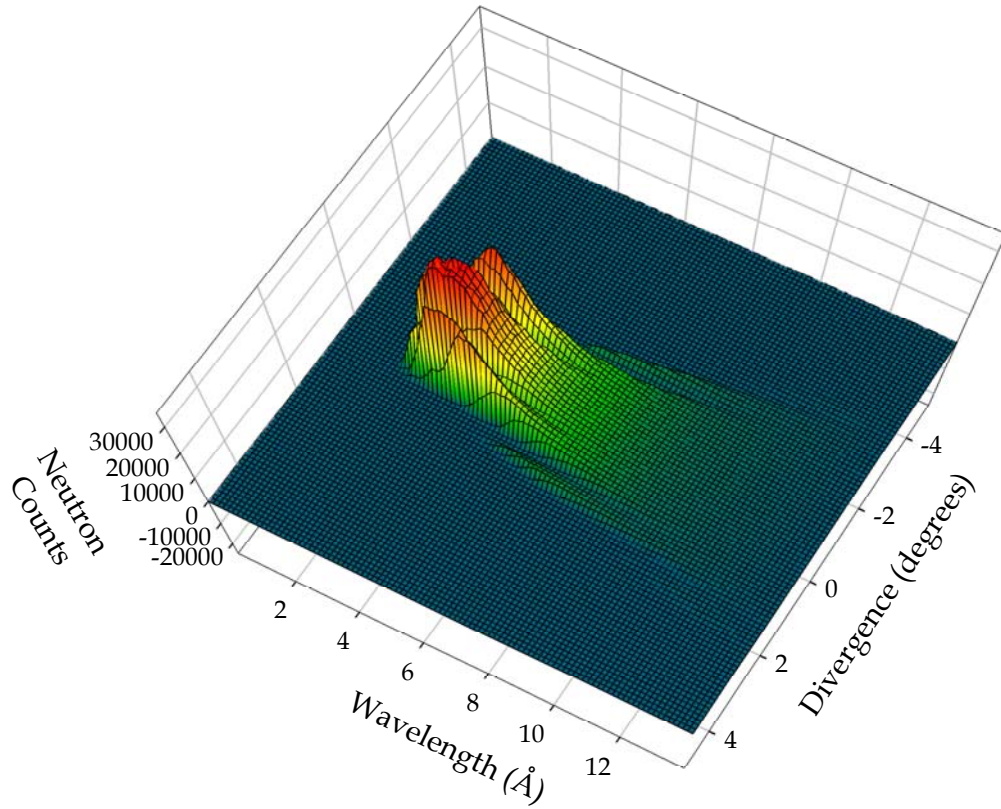


Figure 24. Horizontal beam divergence as a function of wavelength for P212

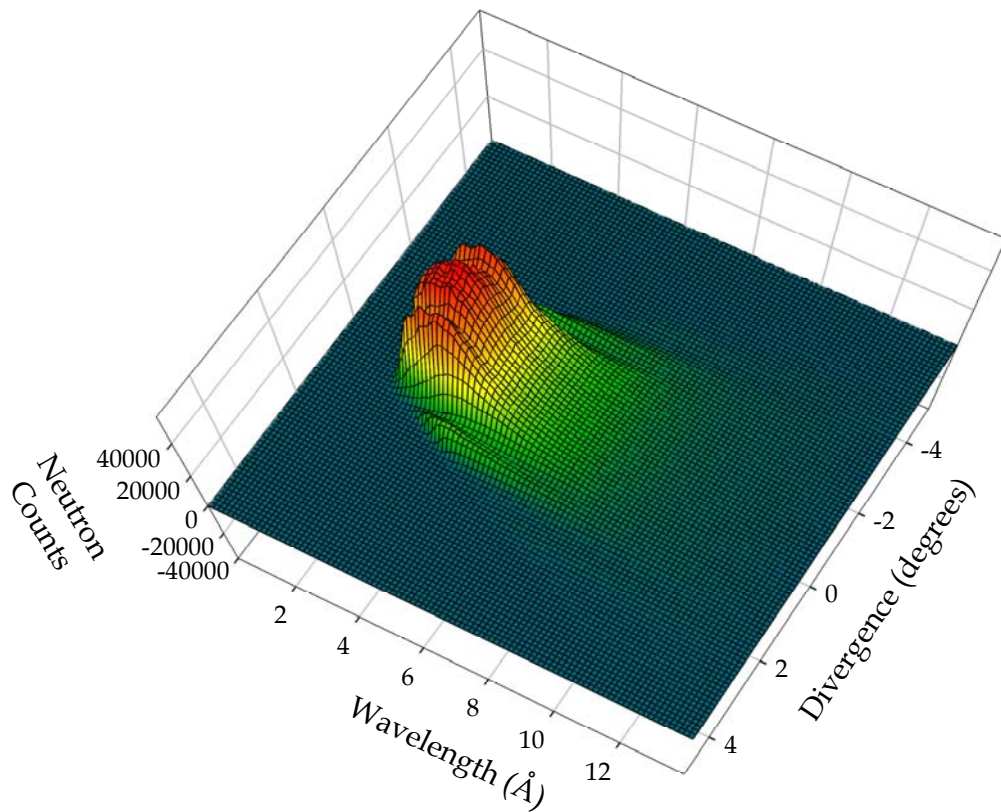


Figure 25. Horizontal beam divergence as a function of wavelength for P353535

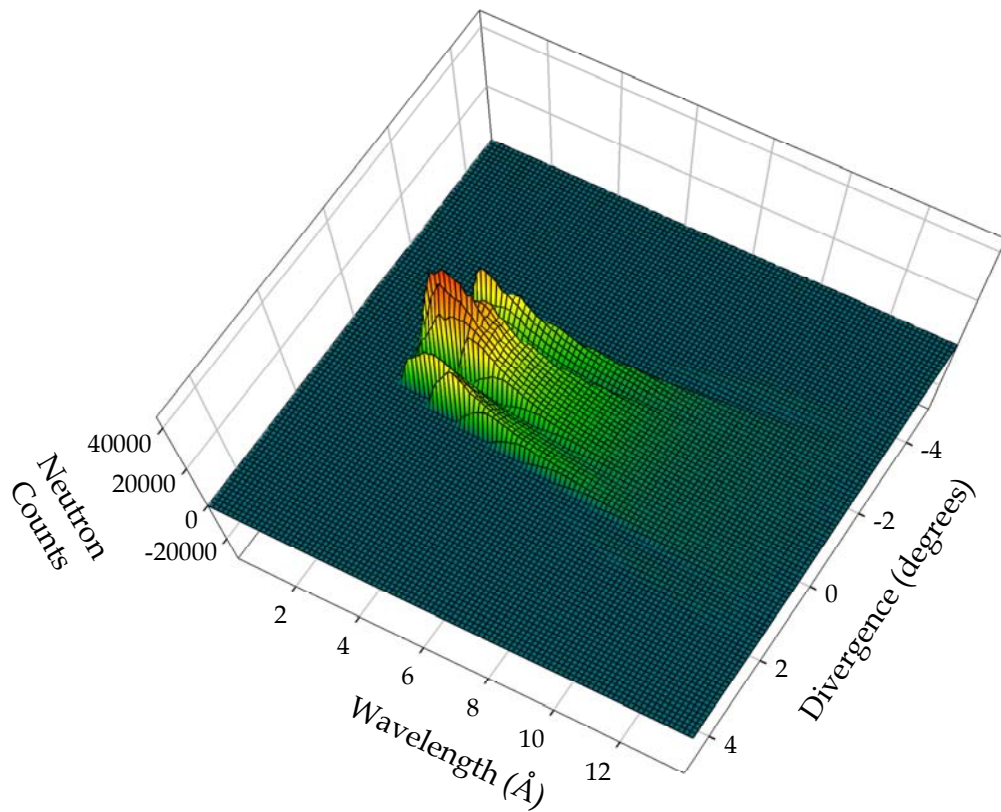


Figure 26. Vertical beam divergence as a function of wavelength for P212

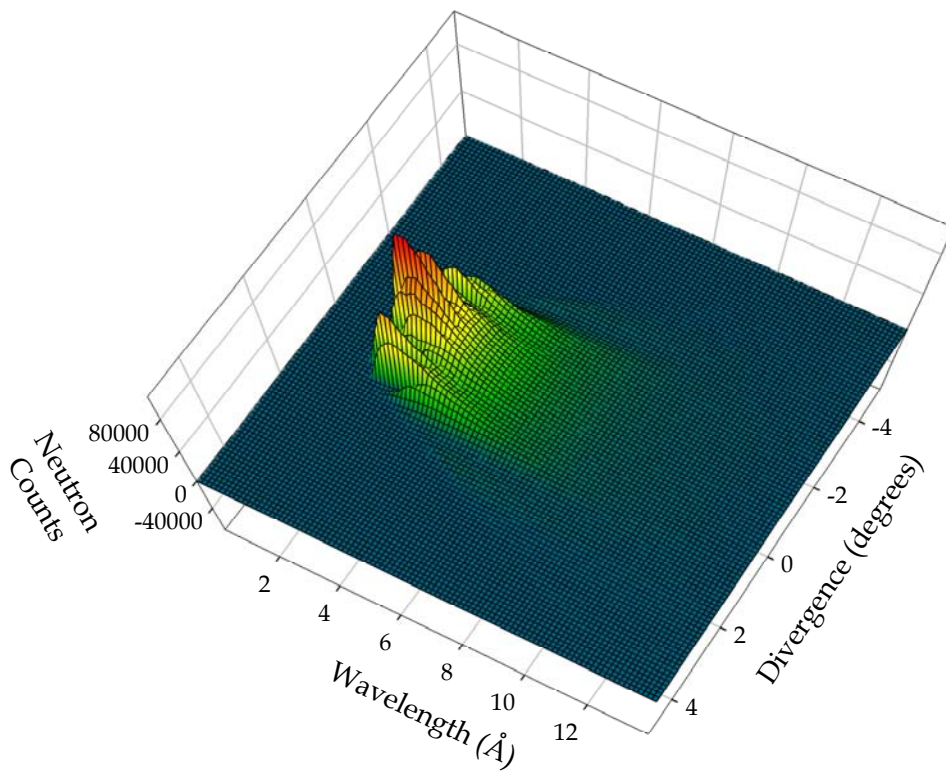


Figure 27. Vertical beam divergence as a function of wavelength for P353535

## Complete Instrument Simulations

For the same configurations shown in the primary instrument simulations the PG002 elastic line has been simulated. The results are shown in figures 28 and 29.

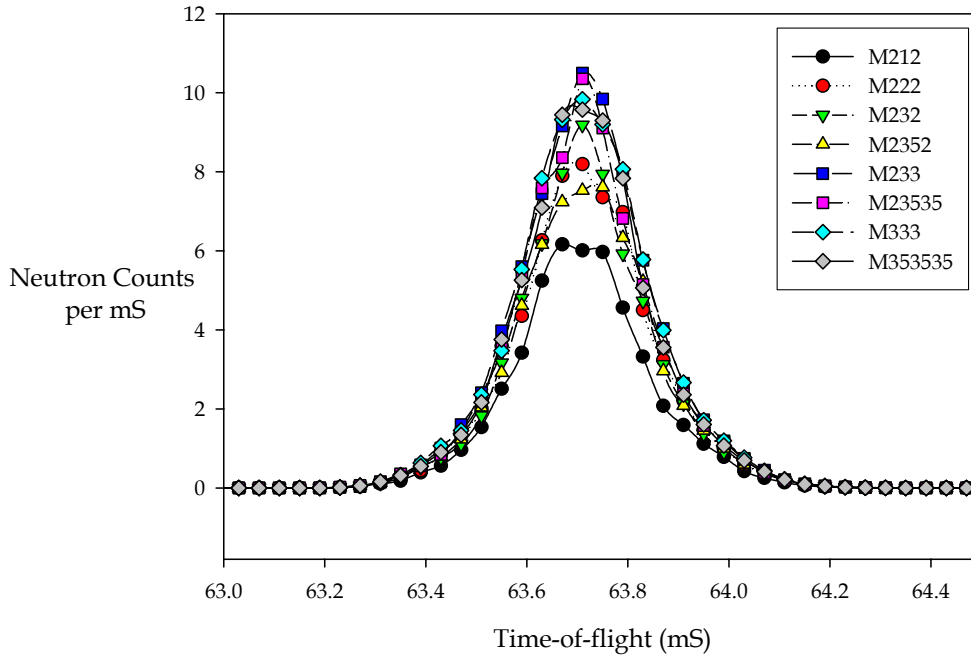


Figure 28. PG002 elastic line intensities for the different guide configurations

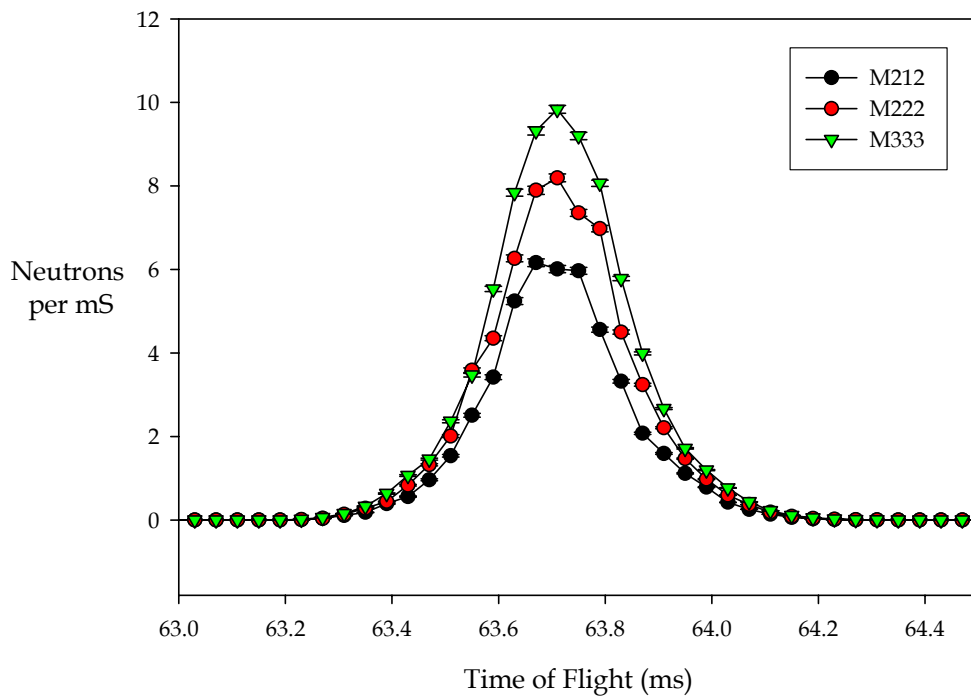


Figure 29. Some configurations in close-up

Clearly, the gains at this wavelength (6.7 Å) are lower than expected and this must be related to the increased beam divergence and beam-size. The larger vertical beam divergence in particular will have an impact on the capability of the analyser to focus the beam down to the detector position – particularly as it is currently not optimized to do this. This does not appear, however, to have a significant impact on the instrumental resolution.

## Speed of simulations

The simulations of the complete instrument are very cpu intensive. Using higher m-factor supermirrors leads to more neutrons reaching later stages of the simulation and so the simulation time must increase and not necessarily in a linear fashion. A  $3 \times 10^9$  neutron trajectory simulation of the M353535 configuration took 66 hours on a 3 GHz equivalent machine. This is a major limiting factor in the number of different simulations that can be performed in a reasonable amount of time.

The use of multiple processors to increase the rate at which computations are performed is becoming more commonplace. Using the power of a PC cluster enables very large computations to be performed in realistic timescales. This can also be applied to instrument simulations. The problem of implementing Vitess on a GRID system has been addressed and solved leading to a factor of 11 improvement (with potentially 15-16) in the speed at which these calculations can be done. Figure 30 shows a screenshot of the grid version of Vitess which is called +Vitess (plus Vitess). A comparison of the output for identical simulations shows that the same statistical accuracy can be attained in a fraction of the time (real time not cpu time). The results of this work will be written up separately.

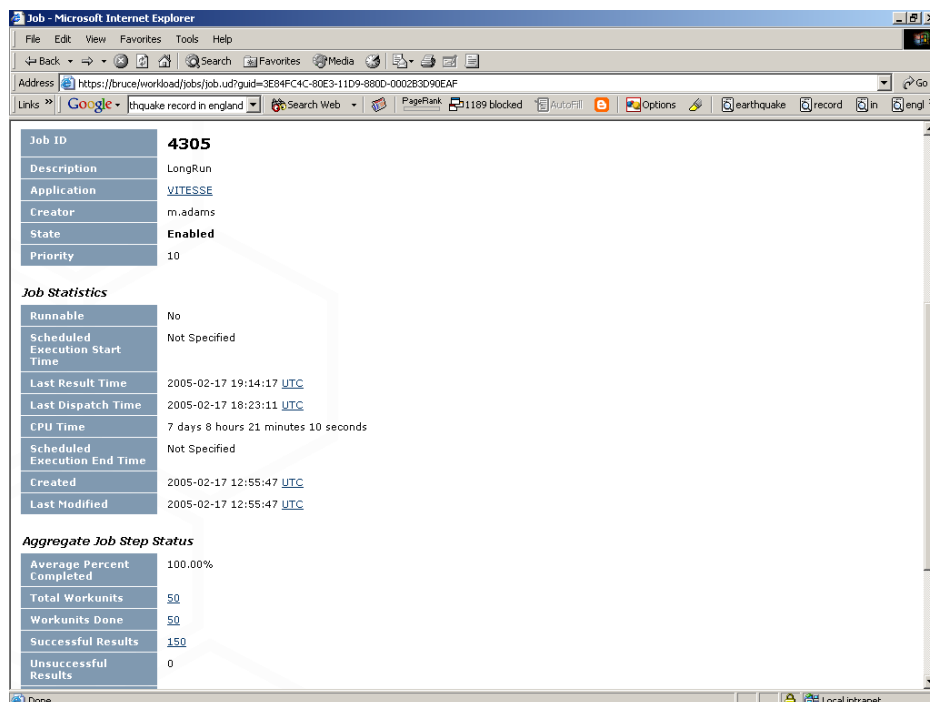


Figure 24. +Vitess in action

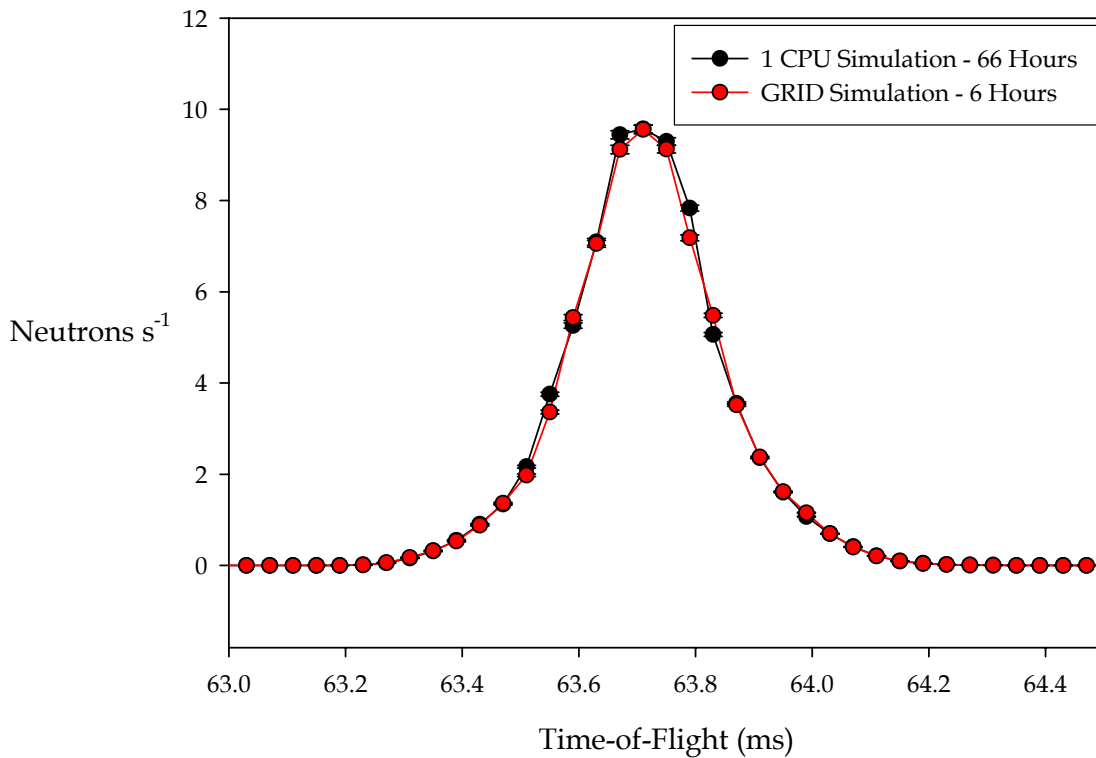


Figure 31. M353535 simulation performed on a single processor and on the Grid.

## Conclusions

The main results of the primary spectrometer simulations are as follows:

1. It is pointless to improve the m-factor of one section of guide and then follow it with a lower m-factor. All gains are lost.
2. When considering the higher m-factor configurations the reflectivity profiles within Vitess play a major role. So, for example, the P333 and P233 configurations outperform the P353535 configuration because the reflectivity of the m=3.5 guide is lower than that of the m=2 and m=3 guides for much of the range of interest. A better optimised m=3.5 guide coating would address this issue.
3. An important factor to consider is that modifying the insert guide within the target station is a much more difficult (and expensive) task than simply changing the guides external to the target station shielding. Thus the fact that the P233 configuration produces very similar flux gains to the P333 configuration is important.

The complete instrument simulations demonstrate the following:

1. The increasing the beam divergence due to the use of higher m-factor mirrors does not just impact on the angular resolution of the spectrometer (as is normally expected) but also on the real detected count-rate as well.

2. Although a gain of  $\sim 2.5$  in the flux of  $6.7\text{\AA}$  neutrons arriving at the sample is possible the increase in detected neutron flux is only  $\sim 1.6$ .
3. Beam divergence is much more pronounced at longer wavelengths. Therefore the reduction in detected neutron flux will be more apparent on the high resolution mica analyser reflections, particularly the important 002 reflection.
4. The use of supermirror guides will have the greatest impact on the flux of higher-energy neutrons in the 10-20meV range. This will be of great benefit for studies of molecular hydrogen.

## Recommendations

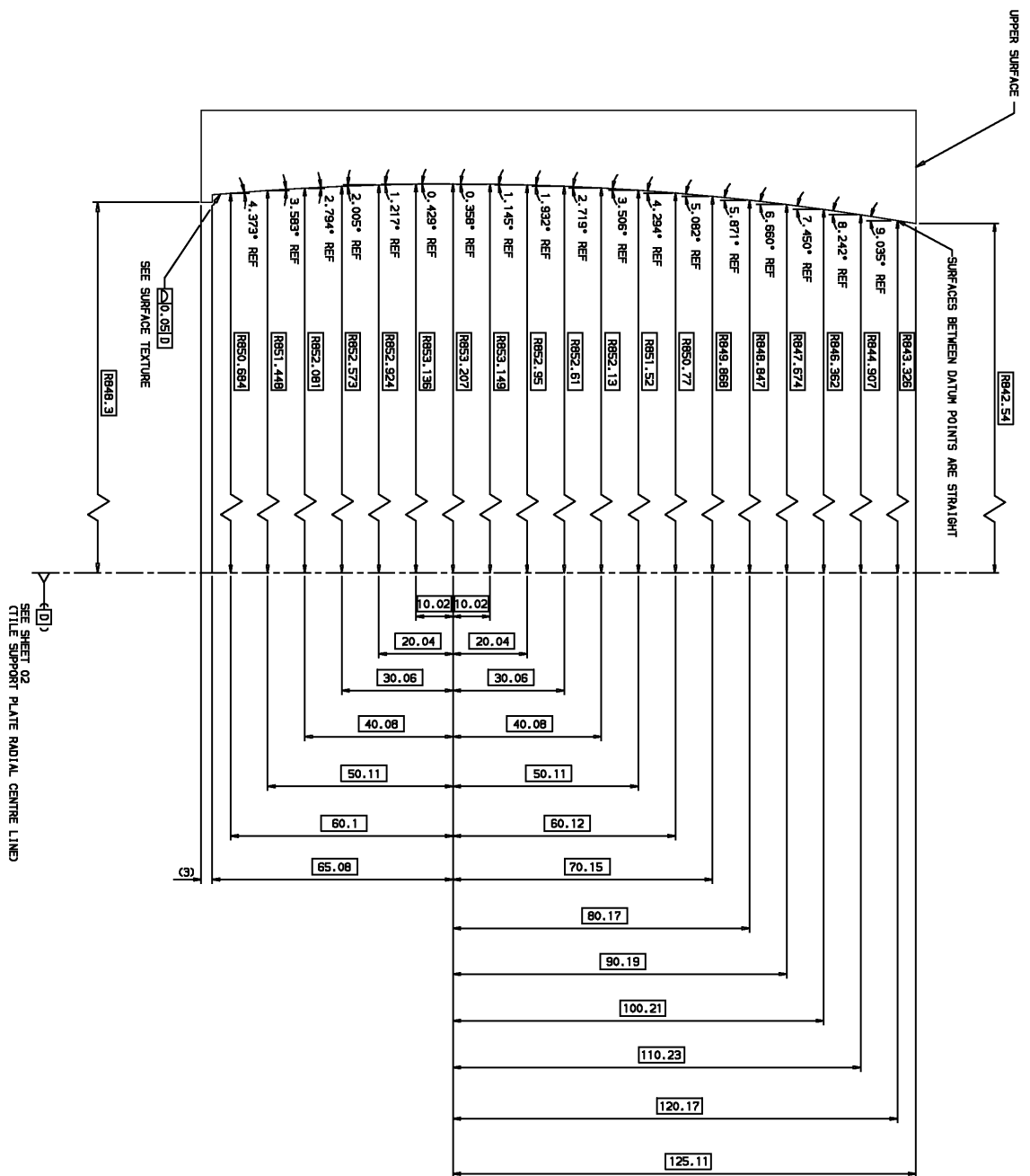
The optimisation of the graphite analyser profile and detector bank should be re-done and steps taken to rectify the current mismatch between these two components of the spectrometer. Further simulation work is required to quantify the effect of beam divergence on both the angular resolution of the spectrometer and the detected neutron gains at mica analyser wavelengths. In addition, the use of parabolic converging guides which are known to reduce beam divergence<sup>21</sup> should also be investigated. If the simulations suggest that this is the case then this would make the decision to install supermirror guides relatively straightforward i.e. without an increased beam divergence the calculated gains in the neutron flux incident on the sample will map onto similar gains in the detected neutron flux.

At shorter wavelengths where the increase in beam divergence is less noticeable it is already clear that the installation of supermirror guides will have a tremendous impact on the quality of science done on IRIS, in particular the newly-discovered capability to study molecular hydrogen.

## References

- 1 C. J. Carlile and M. A. Adams, *Physica B* **182**, 431-440 (1992).
- 2 M. A. Adams, RAL-TR-97-052 (1997).
- 3 M. A. Adams, F. Fernandez-Alonso et al. , RAL-TR-2004-022 (2004).
- 4 D. M. Marero and D. Engberg, *Physica B* **268**, 134-138 (1999).
- 5 D. M. Y. Marero, in *European Powder Diffraction, Pts 1 and 2; Vol. 321-3* (2000), p. 290-295.
- 6 D. M. Y. Marero et al. , *Physica B* **276**, 150-151 (2000).
- 7 D. M. Y. Marero, *Applied Physics A* **74**, S289-S291 (2002).
- 8 D. Wechsler, G. Zsigmond, and F. Streffer, *Neutron News* **11**, 25-28 (2000).
- 9 K. Lefmann and K. Nielsen, *Neutron News* **10**, 20 (1999).
- 10 K. Lefmann et al. , *Physica B* **152**, 276-278 (2000).
- 11 G. Zsigmond and F. Mezei, *Physica B* **276**, 106-107 (2000).
- 12 C. J. Carlile, *Physica B* **266**, 131-137 (1999).
- 13 M. T. F. Telling, RAL-TR-2004-021 (2004).
- 14 C. Schanzer et al. , *Nuclear Instruments & Methods in Physics Research Section A* **529**, 63-68 (2004).
- 15 T. Hils et al. , *Physica B-Condensed Matter* **350**, 166-168 (2004).
- 16 M. W. Johnson, RL-80-065 (1980).
- 17 M. W. Johnson and C. Stephanou, RL-78-090 (1978).
- 18 S. I. Campbell, M. T. F. Telling, and C. J. Carlile, *Physica B* **276**, 206-207 (2000).
- 19 M. T. F. Telling and S. I. Campbell, RAL-TR-1999-044 (1999).
- 20 S. I. Campbell, (2004).
- 21 L. C. Chapon, (2005).





# Appendix B. Screenshots of the ViteSS GUI

The image shows two screenshots of the ViteSS 2.5.1 GUI. The top screenshot is the 'Instrument IRRS' configuration window, and the bottom screenshot is the 'Edit ls1st51hydrogen.mod' dialog box.

### Instrument IRRS Configuration

**File Edit Configure Tools Options Help**

**VITESS 2.5.1**

Click parameter names for help!

**Check**

**Start**

**Kill**

**Stop**

**Module 1 source\_SIS-1**

1  2  3  4  5  6  7  8  9  10  11  12  13  14  15  16  17  18  19  20  21  22  23  24

source\_SIS-1

guide

chopper\_disc

guide

chopper\_disc

guide

guide

space

nonz\_pos

sample\_elasticisor

nonz\_pos

ma\_focus\_dat

nonz\_pos

space

nonz\_pos

space

nonz\_pos

space

nonz\_pos

detector

writout

eval\_inclust

---inactive---

**Restriction of sampling trajectories**

number of trajectories [1000000]

min. time [ms] [0]  max. divergence X <-> Y [deg] [0.5]

max. wave length [Å] [6.9]  max. divergence X <-> Z [deg] [0.5]

direction defined by window

degree of polarization [0]

propagation Y [0]  Z [0]

diameter to window [53.3]  width [cm] [4.5]  height [cm] [6.7]

declination [13]

**Special simulation parameters**

time of measurement [s]

retracting file

kind of raytracing

### Edit ls1st51hydrogen.mod

**Moderator 1**

moderator type

shape

diameter [11]  moderator height [cm] [12]

center of moderator X [cm] [0]  center Y [cm] [0]  center Z [cm] [0]

total flux at moderator [1e18]  neutron current [n/s] [0]

user wavelength [Å]  colour [0]

moderator temperature [K] [25]

user wavelength [Å]  ViteSS

moderator temperature [K] [25]

tau\_1 [µs] [0]  tau\_2 [µs] [0]

user time  moderator dist. file

tau\_1 [µs] [0]  tau\_2 [µs] [0]

user time  moderator dist. file

**Moderator 2**

moderator type

shape

diameter of moderator [cm] [0]  moderator height [cm] [0]

center of moderator X [cm] [0]  center Y [cm] [0]  center Z [cm] [0]

total flux at moderator [n/(cm²s)]  neutron current [n/s] [0]

user wavelength [Å]  colour

moderator temperature [K] [0]

user wavelength [Å]  ViteSS

moderator temperature [K] [0]

tau\_1 [µs] [0]  tau\_2 [µs] [0]

user time  moderator dist. file

tau\_1 [µs] [0]  tau\_2 [µs] [0]

user time  moderator dist. file

input file

output file

parameter directory

random seed  min. neutron weight  gravity on

Module 13 ma\_focus.dat  
Monochromator Analyser

parameter file

focus file

repetition rate  mosaic spread  mosaic spread horiz. [deg]  mosaic spread vert. [deg]

d spread  reflectivity normalization [-]

d-distribution

1 source\_ISTS-1

2 guide

3 chopper\_disc

4 guide

5 chopper\_disc

6 guide

7 guide

8 guide

9 space

10 mon2\_pos

11 sample\_elastic\_isostr

12 mon2\_pos

13 ma\_focus.dat

14 mon2\_pos

15 space

16 mon2\_pos

17 space

18 mon2\_pos

19 space

20 mon2\_pos

21 detector

22 writout

23 eval\_inelast

24 --inactive--

**Edit analyser\_iris.crs**

Monochromator-Analyser parameters

main position X [cm]	<input type="text" value="85.002"/>	main position Y [cm]	<input type="text" value="0"/>	main position Z [cm]	<input type="text" value="0"/>
surface offset horizontal [deg]	<input type="text" value="0"/>	surface offset vertical [deg]	<input type="text" value="3.9"/>	Bragg offset horizontal [deg]	<input type="text" value="3.9"/>
Bragg offset vertical [deg]	<input type="text" value="0"/>	thickness cryst. element [cm]	<input type="text" value="0.1"/>	width cryst. element [cm]	<input type="text" value="1"/>
d-spacing [Å]	<input type="text" value="3.3291"/>	order of reflection	<input type="text" value="1"/>	height cryst. element [cm]	<input type="text" value="1"/>
mosaic range factor	<input type="text" value="1000"/>	d-range factor	<input type="text" value="5"/>		

Output frame

output frame definition user defined frame

X' [cm]	<input type="text" value="85.002"/>	Y' [cm]	<input type="text" value="0"/>	Z' [cm]	<input type="text" value="0"/>
horizontal angle [deg]	<input type="text" value="180"/>	vertical angle [deg]	<input type="text" value="5.4"/>		